

# The Evolutionary Status of Be Stars: Results from a Photometric Study of Southern Open Clusters

M. Virginia McSwain<sup>1,2</sup>

*Department of Astronomy, Yale University, P.O. Box 208101, New Haven, CT 06520-8101*

mcswain@astro.yale.edu

Douglas R. Gies

*Department of Physics and Astronomy, Georgia State University, P.O. Box 4106, Atlanta, GA 30302-4106*

gies@chara.gsu.edu

## ABSTRACT

Be stars are a class of rapidly rotating B stars with circumstellar disks that cause Balmer and other line emission. There are three possible reasons for the rapid rotation of Be stars: they may have been born as rapid rotators, spun up by binary mass transfer, or spun up during the main-sequence (MS) evolution of B stars. To test the various formation scenarios, we have conducted a photometric survey of 55 open clusters in the southern sky. Of these, five clusters are probably not physically associated groups and our results for two other clusters are not reliable, but we identify 52 definite Be stars and an additional 129 Be candidates in the remaining clusters. We use our results to examine the age and evolutionary dependence of the Be phenomenon. We find an overall increase in the fraction of Be stars with age until 100 Myr, and Be stars are most common among the brightest, most massive B-type stars above the zero-age MS (ZAMS). We show that a spin-up phase at the terminal-age MS (TAMS) cannot produce the observed distribution of Be stars, but up to 73% of the Be stars detected may have been spun-up by binary mass transfer. Most of the remaining Be stars were likely rapid rotators at birth.

Previous studies have suggested that low metallicity and high cluster density may also favor Be star formation. Our results indicate a possible increase in the fraction of Be stars with increasing cluster distance from the Galactic center (in environments of decreasing metallicity). However, the trend is not significant and could be ruled out due to the intrinsic scatter in our data. We also find no relationship between the fraction of Be stars and cluster density.

*Subject headings:* stars: emission-line, Be — open clusters and associations: individual (Basel 1, Bochum 13, Collinder 272, Haffner 16, Hogg 16, Hogg 22, IC 2395, IC 2581, IC 2944, NGC 2343, NGC 2362, NGC 2367, NGC 2383, NGC 2384, NGC 2414, NGC 2421, NGC 2439, NGC 2483, NGC 2489, NGC 2571, NGC 2659, NGC 3293, NGC 3766, NGC 4103, NGC 4755, NGC 5281, NGC 5593, NGC 6178, NGC 6193, NGC 6200, NGC 6204, NGC 6231, NGC 6249, NGC 6250, NGC 6268, NGC 6322, NGC 6425, NGC 6530, NGC 6531, NGC 6604, NGC 6613, NGC 6664, Ruprecht 79, Ruprecht 119, Ruprecht 127, Ruprecht 140, Stock 13, Stock 14, Trumpler 7, Trumpler 18, Trumpler 20, Trumpler 27, Trumpler 28, Trumpler 34, vdB-Hagen 217)

## 1. Introduction

Be stars are well known to be a class of rapidly rotating stars (Slettebak 1949, 1966; Slettebak et al. 1992). Slettebak (1966) showed that the ob-

---

<sup>1</sup>Visiting Astronomer, Cerro Tololo Inter-American Observatory. CTIO is operated by AURA, Inc. under contract to the National Science Foundation.

<sup>2</sup>NSF Astronomy and Astrophysics Postdoctoral Fellow

served equatorial rotational velocities,  $v_{rot}$ , of Be stars are 70%–80% of the critical breakup velocity,  $v_{crit}$ , although Townsend, Owocki, & Howarth (2004) and Frémat et al. (2005) showed that observed Be star rotational velocities may be systematically underestimated due to the effects of gravitational darkening on spectral lines. Therefore Be stars may rotate much closer to their critical velocities than the available observations suggest. This rapid rotation may be combined with weaker processes, such as non-radial pulsations or magnetic fields (Porter & Rivinius 2003), to move material from the stellar surface into a disk (Townsend et al. 2004).

There are three possible reasons for the rapid rotation of Be stars: they may have been born as rapid rotators, spun up by binary mass transfer, or spun up during the MS evolution of B stars. Many authors (Mermilliod 1982; Grebel 1997; Zorec & Briot 1997; Fabregat & Torrejón 2000) have found the highest fractions of classical Be stars among spectral types B0–B2, appearing most often between the ages 13 – 25 Myr (Fabregat & Torrejón 2000). Fabregat & Torrejón use these results to argue that the Be phenomenon is due to an evolutionary spin-up among B-type stars towards the end of the MS lifetime (Meynet & Maeder 2000; Keller et al. 2001). On the other hand, Abt (1979) found no dependence on the Be frequency with age, and Mermilliod (1982) and Slettebak (1985) noted that Be stars are found throughout the entire MS band, from the ZAMS through the TAMS, indicating that Be stars can occur at any age. Therefore it is also possible that the evolution of close binary systems may lead to mass transfer onto B stars, thereby increasing their angular momentum and inducing disks (Pols et al. 1991). Finally, Zorec & Briot (1997) find constant fractions of Be stars with luminosity class, and they argue that the Be phenomenon is not associated with a particular evolutionary phase. Rather, it is more likely due to rapid rotation in B stars at the time of their formation. Because these various studies disagree about the relationship between the Be frequency and evolution, further investigations are necessary to resolve the issue.

Therefore we present here an extensive photometric survey of open clusters to study their Be star populations. Our detection technique is demonstrated for the cluster NGC 3766 in Mc-

Swain & Gies (2005), hereafter referred to as Paper 1. In this paper we present photometric data for 55 open clusters, and we identify a total of 52 definite Be stars and 129 Be star candidates in the 48 reliable open clusters. We use our sample of Be stars to conduct a statistical analysis of the Be phenomenon and explore the reasons for their rapid rotation.

## 2. Observations and Data Analysis

We selected the target open clusters for this study using the WEBDA database<sup>3</sup>. We chose clusters with ages between 1–32 Myr,  $V - M_V < 13$ , and angular diameters between 5–20". However, we also included some older clusters to improve our statistics, and many of the ages and distance moduli from WEBDA were later revised using other references. We restricted our targets to clusters in the southern sky; all have declination  $< 0^\circ$ . To eliminate clusters with obvious associated nebulosity, we used the Space Telescope Science Institute (STScI) Digitized Sky Survey<sup>4</sup> to view a red image of each cluster. While the requirement of little to no nebulosity reduced the difficulty of the photometry, it did eliminate many very young clusters from our sample.

We made photometric observations of the clusters over 14 nights between 2002 March 27 – April 2 and 2002 June 19 – 25 with the CTIO 0.9m telescope and SITe 2048 CCD. The images were binned using a CCD summing factor of 2 pixels  $\times$  2 pixels due to the slow readout time of the chip. Without binning, the chip has a plate scale of 0".401 pixel<sup>-1</sup>, but with binning the plate scale increased by a factor of 2.

Most clusters were observed at least twice in each of the Strömgren  $b$  and  $y$  filters as well as a narrow band  $H\alpha$  filter, and the exposure times usually varied from 5–120 s duration depending on the brightness of the cluster. During the 2002 March run, we also observed five standard stars from the list of Cousins (1987): HD 79039, HD 80484, HD 104664, HD 105498, and HD 128726. We observed the standard stars HD 105498, HD

<sup>3</sup>The WEBDA database is maintained by J.-C. Mermilliod and is available online at [obswwww.unige.ch/webda/navigation.html](http://obswwww.unige.ch/webda/navigation.html).

<sup>4</sup>The STScI Digitized Sky Survey is available online at [http://stdatu.stsci.edu/cgi-bin/dss\\_form](http://stdatu.stsci.edu/cgi-bin/dss_form).

128726, HD 156623, HD 157795, HD 167321, and HD 216743 from the lists of Cousins (1987) and Clausen et al. (1997) during the 2002 June nights. Unless the weather prohibited observations, each standard star was observed in each band at a minimum of three different airmasses. All of the images were processed in IRAF<sup>5</sup> using nightly bias and dome flat frames.

The photometry of each standard star and cluster was measured and calibrated according to the methods discussed in Paper 1. We measured the errors in the magnitudes by combining the estimated instrumental errors, the standard deviation of the aperture correction, and the errors in the transformation coefficients, and these quantities vary for each cluster due to nightly variations in atmospheric conditions and the exposure time used. From our images, we also performed astrometry of the clusters according to the technique described in Paper 1, and the errors are typically less than  $0''.10$  in both  $\alpha \cos \delta$  and  $\delta$ . However, several clusters did not fit into a single field of view, and they were observed in three or four fields. These clusters are Collinder 272, Hogg 16, IC 2395, NGC 2343, NGC 6425, NGC 6531, Stock 13, and Trumpler 18. The astrometry errors of these clusters are larger, but usually less than  $0''.50$  in both  $\alpha \cos \delta$  and  $\delta$ .

Our photometry and astrometry of each star in the 55 clusters are listed in Table 1, available online (see Note to Table 1). Although we often exclude stars near the edge of the CCD or near bad columns, the photometry of each open cluster is usually complete enough to include all of its (unsaturated) OB stars. It is complete to  $y = 13$  for the brightest clusters, but we obtained deeper images and measured magnitudes up to  $y = 17$  in some cases.

From the calibrated photometry, we created  $(b-y, y)$  color-magnitude and  $(b-y, y-H\alpha)$  color-color diagrams like those described in Paper 1 for NGC 3766. Because the MS of the  $(b-y, y)$  diagram is nearly vertical in the region of massive OB stars, it was very difficult to constrain the distance modulus and the age of each cluster. Therefore,

to determine the cluster parameters ( $E(B-V)$ ,  $V_0 - M_V$ , and age), we searched the available literature for the various values for each cluster. We used these values to plot the theoretical isochrones from Lejeune & Schaerer (2001) and theoretical color-color curve using colors derived from Kurucz (1979) model spectra. This technique is described for NGC 3766 in Paper 1. The Lejeune & Schaerer (2001) isochrone models do not provide Strömgren magnitudes, so we transformed the Johnson  $V$  and  $B$  magnitudes to the Strömgren system using the transformations

$$y = V - 0.038(B - V) \quad (1)$$

(Cousins & Caldwell 1985) and

$$B - V = 1.584(b - y) + 0.681m_1 - 0.116 \quad (2)$$

(Turner 1990), as described in Paper 1. We also transformed  $E(B-V)$  to  $E(b-y)$  using the relationship

$$E(b-y) = 0.745 E(B-V) \quad (3)$$

from Fitzpatrick (1999), assuming  $R \equiv A(V)/E(B-V) = 3.1$ . In very few cases, a cluster did not have published parameters available, or the published values did not agree well with our observations, so we fit our data to the theoretical curves using a grid of values for  $E(b-y)$ ,  $V_0 - M_V$ , and  $\log$  age. For all clusters, we retained the parameters that resulted in the best fit between our data and the theoretical curves, and the resulting parameters are listed in Table 2. Our technique to select definite and possible Be stars from the normal B stars in our images according to their excess brightness in the narrow band  $H\alpha$  filter is described in Paper 1, and Table 2 also includes the numbers of Be and B stars identified in each cluster.

### 3. Results from Photometric Study

Before we consider the results from this photometric survey, it is important to review the errors inherent in this study. Saturated stars affect the number of very bright B and Be stars that we detect, but this problem is ameliorated by the availability of data on most bright cluster members in the literature. However, we do not include saturated stars in the number of Be and B stars in Table 2. A second problem is that our photometry

<sup>5</sup>IRAF is distributed by the National Optical Astronomy Observatory, which is operated by the Association of Universities for Research in Astronomy, Inc., under cooperative agreement with the National Science Foundation.

technique only detects those Be stars that had active H $\alpha$  emission at the time of our observations, so we detect only the lower limit of the true Be population. We showed in Paper 1 that the true fraction of Be stars is probably between 1.2 – 2.3 times the number detected. Assuming that the ratio of active to inactive Be stars is similar among different clusters, the neglect of inactive Be stars will have no impact on our statistical comparison of the Be star frequency between clusters. The largest source of errors in our study is due to the difficulty detecting weakly emitting Be stars since the errors in their photometry are comparable to the strength of their emission. There is also a possibility that unreddened foreground stars or, less often, background supergiants, contaminate the MS and appear as weak emitters in the color-color diagram. Field stars cause special problems for the five targets that are not truly bound clusters, and the ages, reddening, and distance moduli for these groups are not representative of the entire stellar population. Finally, one of our requirements for identifying B-type stars (see Paper 1) is that  $b - y < E(b - y)$ , which neglects the inherent width of the MS, and we may omit some B and Be stars redward of this cutoff. This is especially a problem at the faint end of the B star MS.

Our photometry of six clusters, excluding the less reliable clusters Bochum 13 and Trumpler 27, did not cover the entire range of B star magnitudes so the total number of B stars in these clusters is underestimated in Table 2. We show below that the number of Be stars omitted is negligible, in agreement with the results of Keller et al. (2001). However, we account for the missing late B-type stars by computing the mass function,  $\xi(\log M)$ . The Lejeune & Schaerer (2001) isochrones assign a mass to each point along the curve, and we interpolated to convert the observed  $y$  magnitudes of the B stars to  $M$ . For the allowed mass range of B-type stars, we binned the stars according to  $\log M$  and counted the unnormalized number,  $N$ , in each bin. The slope of the linear fit between  $\log N$  and  $\log M$  provides  $\Gamma$ , where

$$\Gamma = d \log \xi(\log M) / d \log M. \quad (4)$$

In the fit, each value of  $N$  was weighted according to  $N^{1/2}$ , which decreases the dependence on the less common high mass stars, and the incomplete lower mass bins were excluded entirely. The aver-

age  $\log M$  in each bin was used to compute the total number of B-type stars expected,  $N_{tot}$ . We calculated  $\Gamma$  and  $N_{tot}$  using 6 – 15  $\log M$  bins, equally spaced along the MS curve in the color-magnitude diagram. Table 3 provides  $\Gamma$ ,  $N_{tot}$ ,  $N_{missing}$ , and the observed mass range of B-type stars,  $\Delta M$ , for the six clusters analyzed. This mass range varies depending on the cluster age, and the upper mass limit is comparable to the observed maximum B star mass in each cluster. The minimum mass of B stars is  $2.3 M_{\odot}$  from the Lejeune & Schaerer (2001) models. We found a slight dependence between  $\Gamma$  and the number of bins used, and the errors for  $\Gamma$  and  $N_{tot}$  reflect the  $1\sigma$  variance. Our values for  $\Gamma$  are consistent with the values for massive stars in open clusters found by Massey et al. (1995).

In this study, we find a total of 52 definite Be stars and an additional 129 possible Be stars in 48 clusters. (Hereafter we ignore the regions that are not true open clusters as well as Bochum 13 and Trumpler 27, discussed in Appendix A.) We also detect 2210 B-type stars, including the Be stars, and we estimate from the clusters' mass distributions that 328 B-type stars are missing from our sample. Considering only the definite Be stars in these clusters, the mean percentage of Be stars is only 2.0%. Including the possible Be stars raises the mean percentage to 7.1%. This is much lower than expected; Abt (1987) found that 18% of field B0 to B7 III-V stars in the Bright Star Catalogue (BSC; Hoffleit & Warren 1991) were classified as Be stars in the literature. However, our study accurately accounts for the total number of B stars within the cluster volume, while Abt's magnitude-limited survey is biased towards early B stars that are probably more rich in Be stars (e.g. Mermilliod 1982). Furthermore, many of the B stars in the BSC are members of the Gould Belt, which has  $7.4 < \log \text{age} < 7.8$  (Perrot & Grenier 2003) and coincides with a maximum in the Be star fraction (see Figure 5 below). This may explain the unusual richness of Be stars in the BSC.

Using our extensive sample of Be stars, we investigate several factors that may influence the population of Be stars in open clusters, beginning with metallicity. Using clusters within the same age interval in the interior and exterior of the Galaxy, the Large Magellanic Cloud (LMC), and the Small Magellanic Cloud (SMC), Maeder,

Grebel, & Mermilliod (1999) found that the ratio of Be stars decreases sharply with increasing metallicity. However, Keller, Wood, & Bessell (1999) found no difference in the fraction of Be stars in the LMC and SMC, although there is a factor of two difference in their metallicities. To look for this influence in our data, we investigated the distribution of the target clusters in the Galactic plane. We calculated the distance of each cluster from the Galactic center,  $d_{cent}$ , using  $R_0 = 8000$  pc as the Sun’s distance from the Galactic center and assuming that each cluster lies within the plane of the Galaxy (valid since all have  $|b| < 6^\circ$ ). The Galactic longitude,  $\ell$ , latitude,  $b$ , distance from the Sun,  $d_\odot$ , and  $d_{cent}$  for each cluster are listed in Table 4. The spatial distribution of clusters with respect to the Sun and the Galactic center is illustrated in Figure 1.

The numbers of definite and possible Be star detections from our photometry are included in Table 2, and we plot the percentage of Be stars as a function of distance from the Galactic center in Figure 2. The diamonds are the lower limits of the Be star fraction, determined from the number of definite detections, and the upper limit assumes that all of the possible candidates are in fact Be stars. Note that this upper limit does not represent the formal error in our measurement, which can be significant in clusters with few B-type stars (especially NGC 6268, in which we find that one of its two B stars is a Be star). For the 35 clusters with  $d_{cent} < R_0$ , the mean Be star population is 1.8%–6.5%. The outer 13 clusters have a mean population of 3.3%–10.5%. Using the Galactic metallicity gradient  $\Delta Z/\text{kpc} = -0.0019$  to  $-0.0029$  (Maeder et al. 1999), over the 4.3 kpc range in distance from the Galactic center,  $\Delta Z = .0082 - .0125$ . Interpolating from Maeder et al., the fraction of Be stars in our clusters should increase by a factor of  $\approx 2$  over this range in metallicity. The mean Be star populations do increase slightly over this distance, but Figure 2 does not provide compelling evidence supporting a dependence on the Galactic Be star fraction with metallicity.

The number of Be stars may also be related to the stellar density in the cluster. Strom, Wolff, & Dror (2005) suggest that the average rotational velocity is greater for higher density clusters, presumably allowing more Be stars to form. They

show that the average rotational velocity of unevolved B stars in the dense clusters  $h$  and  $\chi$  Persei is more than  $2\times$  that of field stars of comparable ages. To investigate the role of the stellar density in each cluster, we calculated the mean B star density of the clusters. We determined the cluster center using the mean positions of the B-type stars, and the standard deviation of the B star positions relative to the cluster center defines the radius of the assumed spherical volume. However, the cluster NGC 6268 has only two B stars, so we used the mean distance from the cluster center to define the radius in this case. We plot the percentage of Be stars against the number of B stars per cubic parsec in Figure 3. Our data show no correlation between the two.

We also consider the relationship between the number of Be stars in open clusters and the cluster age, a possible signature of evolutionary effects involved in the origin of Be star disks. Past studies have disagreed on the relationship between the ages and numbers of Be stars. Fabregat & Torrejón (2000) found that classical Be stars are most abundant between  $7.1 < \log \text{age} < 7.4$ . On the other hand, Mermilliod (1982) and Slettebak (1985) found a weaker dependence on age. Instead, they noted that Be stars occupy the entire MS band, from the ZAMS through the TAMS, indicating that Be stars occur at any evolutionary stage. Mermilliod (1982) found that the frequency of Be stars depends instead on spectral type; the abundance peaks for types B1–B2 and B7–B8. However, Zorec & Briot (1997) also found no distinct peak the Be star frequency with luminosity class, and they argue that the Be phenomenon is more likely due to the characteristics of B stars at the time of their formation. This would imply a higher fraction of Be stars among young clusters.

We present a plot of the Be star percentage as a function of cluster age in Figure 4. While we did not compute the formal error in the ages, the agreement among different ages provided in the literature and the good match between the theoretical isochrones and our color-magnitude diagrams suggest that the cluster ages are accurate to  $\pm 0.2$  dex in most cases. Because no clear relationship between the percentage of Be stars and the cluster age emerges from Figure 4, we plot the average Be frequency in four age bins in Figure

5. The bins correspond to the ages  $\log \text{age} < 7.0$ ,  $7.0 \leq \log \text{age} < 7.4$ ,  $7.4 \leq \log \text{age} < 8.0$ , and  $\log \text{age} \geq 8.0$ . Our definite Be star frequency and the Poisson errors are plotted using solid lines, and the total of definite and possible Be stars, also with the Poisson errors, are represented with dashed lines. The plotted ages represent the mean age observed within each bin, and the age error bars represent the maximum and minimum ages from our sample. We are surprised to see that the fraction of Be stars is generally highest among clusters with  $7.4 \leq \log \text{age} < 8.0$ , unlike previous studies that found a peak among clusters with  $7.0 \leq \log \text{age} < 7.4$  (Fabregat & Torrejón 2000). Figure 5 reveals that the population of Be stars generally increases with time until  $7.4 \leq \log \text{age} < 8.0$ , then declines among older clusters.

Finally, we plot the 52 definite Be stars in Figure 6 using their intrinsic colors and absolute magnitudes. For comparison, the normal B-type stars are plotted as contours overlying the absolute color-magnitude diagram. To derive the absolute magnitudes, we used the relation

$$A(y) = 3.034 E(B - V) \quad (5)$$

interpolated from Fitzpatrick (1999). The horizontal dashed lines in Figure 6 divide the Be population into four bins: evolved ( $M_y < y_{Bmin}$  at the ZAMS), early B spectral types, mid B stars, and late B stars. The isochrone for  $10^5$  yr represents a very young age, close to the ZAMS, and the isochrones for a distribution of stars with ages of  $10^7$  and  $10^8$  yr are also plotted. Although the Be stars are generally a redder population than the B-type stars (the two most significant outliers to the lower left of the ZAMS are No. 12 in NGC 6531 and No. 355 in Trumpler 34; see discussion in Appendix A), it is unlikely that the Be stars in a given cluster are a more evolved population than their neighboring B stars, and we believe that other effects are largely responsible for their position relative to the ZAMS. The circumstellar disk can impart additional reddening, rotationally induced gravitational darkening may cause them to appear cooler than a non-rotating star of the same mass, or light may be preferentially scattered by the disks and cause the stars to appear brighter and more evolved (Slettebak 1985; Zorec & Briot 1997).

Although Figure 6 reveals that the definite Be stars are rather uniformly distributed in  $M_y$ , the relative fraction of Be and B stars decreases with later spectral types. Be stars comprise a respective 7.4%, 4.7%, 2.1%, and 0.9% of the evolved, early, mid, and late type B stars in our sample. A histogram plot illustrating the relative populations for each bin is shown in Figure 7. These results indicate that the relative fraction of Be stars attains a maximum among the evolved stars that are approaching the TAMS. (Note that these evolved stars do not correspond to the oldest age bin defined above, where a decline in the Be population is observed.) Fabregat & Torrejón (2000) also found that the Be phenomenon occurs during the second half of the MS, which they argue is the result of an evolutionary spin-up as the stars approach the TAMS.

#### 4. Conclusions

Our results indicate that the Be phenomenon is not strongly dependent on metallicity or cluster density, but it is clearly influenced by the evolutionary state of B stars. We observe a higher fraction of evolved Be stars, but if Be stars were born as rapid rotators as believed by Zorec & Briot (1997), the opposite trend would be observed; more Be stars would be observed in unevolved stars, in the youngest clusters, since the rotation rate decreases during the MS lifetime (Meynet & Maeder 2000). Also, Be stars born as rapid rotators would have a much different distribution along the MS. A rotationally distorted star with mass  $M_B$  at the critical breakup velocity will have an equatorial radius

$$R_e = 1.5 \left( 0.914 + \frac{0.143}{(M_B/M_\odot)^2} \right) R_B \quad (6)$$

(Frémat et al. 2005), where  $R_B$  is the radius of a non-rotating B star. The resulting critical breakup velocity is

$$v_{crit} = 436.7 \left( \frac{M_B/M_\odot}{R_e/R_\odot} \right)^{1/2} \text{ km s}^{-1}. \quad (7)$$

Table 5 compares this  $v_{crit}$  with the mean projected rotational velocity,  $\langle v \sin i \rangle$ , of B stars from Abt, Levato, & Grosso (2002). Masses and radii are from Harmanec (1988). Later B-type stars

have a mean rotational velocity closer to their critical value, so that if these velocities reflect their birth spins, then we should expect to see a higher fraction of Be stars among late B stars. We show in Figure 7 that such a distribution is not observed, hence we doubt that many Be stars are born as fast rotators.

Meynet & Maeder (2000) predicted that stars with  $M > 12M_{\odot}$  experience a short spin-up phase at the end of their MS lifetimes, and this spin-up phase could be responsible for the high fraction of evolved Be stars observed in this study. We do not expect an age dependence with this scenario; as long as a cluster has TAMS B stars, Be stars would be expected. However, the duration of this spin-up phase is expected to be short, only about 1% of the MS lifetime, so we should observe a comparable Be star fraction if the TAMS spin-up phase is the origin of the rapid rotation. While lower mass B stars are not expected to experience such a spin-up, Meynet & Maeder (2000) predict that these stars may remain rapid rotators and in fact increase their fraction of the breakup velocity as they evolve along the MS. Once again, this would support a larger fraction of late Be stars, which is not observed.

We find it more likely that Be stars are spun-up by mass transfer in close binary systems. Although there is a perceived deficiency of short period Be star binaries (e.g. Abt & Levy 1978), recent work has led to the discovery of 55 Be star binaries with periods  $< 100$  d (Gies 2000; Raguzova & Popov 2005), and Be stars have been observed in nearly all stages of the proposed binary evolution scenario. The initially more massive star expands to fill its critical Roche lobe during the H shell burning phase, triggering Case B mass transfer and causing the spin-up of the mass gainer (Gies 2000). The massive Algol binary RY Per is an example of such a spin-up process in action; the F7: II-III donor star is engaged in active mass transfer via Roche lobe overflow onto the B4: V companion, and the mass gainer has been spun up to more than seven times faster than the synchronous rate (Barai et al. 2004). Commonly, the mass ratio becomes inverted during the mass transfer and the orbital separation  $a$  increases, leading to a dramatic increase in the timescale for tidal synchronization ( $\sim a^{17/2}$ ; Hilditch 2001). This timescale becomes much longer than the H shell burning

phase, so the mass gainer will retain its rapid rotation long after the mass transfer is complete. At the conclusion of the mass transfer phase, the donor star is left as a stripped down, helium star remnant – a small but hot subdwarf (Gies 2000).  $\phi$  Per is the only confirmed Be+sdO system (Thaller et al. 1995; Gies et al. 1998), but three additional candidates have been identified: 59 Cyg (Maintz et al. 2004), HR 2142 (Waters, Cote, & Pols 1991), and FY CMa (Rivinius et al. 2004). Depending on its mass, the sdO star will eventually become a white dwarf (WD) or explode as a supernova to form a Be + neutron star (NS) binary or an unbound system (Gies 2000). To date, no Be + WD systems are known, but 130 Be/X-ray binaries (presumably with NS companions) have now been identified (Raguzova & Popov 2005).

Pols et al. (1991) and Van Bever & Vanbeveren (1997) predicted that the fraction of mass gainers is highest among B0–B3 stars, decreasing with later spectral types, consistent with the distribution of Be stars that we observe. If the mass transfer is conservative (as expected for systems with a high initial mass ratio,  $q > 0.6$ ), Pols et al. (1991) showed that the mass gainers would be observed as rejuvenated, bright MS stars, including blue stragglers. However, Be stars formed this way may not appear near the ZAMS due to disk reddening and gravitational darkening. On the other hand, Pols et al. showed that there is a minimum  $q$  (between 0.3 – 0.5, depending on their model) for the production of Be stars from close binary evolution with non-conservative mass transfer. Therefore, Be stars formed by mass transfer would be found preferentially in the upper part of the MS.

Previous studies have estimated the percentage of the Be stars that are products of close binary evolution. Pols et al. (1991) predicted that 1.3%–3.9% of B-type stars should be observed as rapid rotators due to angular momentum received during case B mass transfer, and Van Bever & Vanbeveren (1997) predicted a similar number (0.9%–4.8%). While the predicted total number of mass gainers is comparable to the number of Be stars that we observe, not all of these mass gainers are expected to become Be stars. Pols et al. (1991) showed that the predicted number of spun-up B stars in the BSC is 40%–60% of the observed number of Be stars in that sample. However, because not all rapidly rotating B-type stars exhibit the Be

phenomenon, Van Bever & Vanbeveren (1997) argued that Be stars represent about half of the total number of rapidly rotating B stars, so the fraction of Be stars in the BSC formed by mass transfer is closer to 20%. We show above that the fraction of Be stars in the BSC is not representative of the fraction in open clusters, so the estimate of Van Bever & Vanbeveren (1997) cannot be applied to our sample, and there is no spectroscopic survey in the literature that provides relative numbers of Be stars and normal, rapidly rotating B stars.

In lieu of an accurate theoretical prediction, we can estimate the fraction of mass gainer Be stars from our results. We plot the observed  $M_y$  of our definite Be stars versus their age in Figure 8. Using the isochrone models of Lejeune & Schaerer (2001), we determined the mass of a primary at the TAMS and its  $M_y$  (dashed curve) over a range of cluster ages. For a close binary system with  $q \approx 1$  and the primary at the TAMS, the mass transfer will be conservative (Pols et al. 1991) and the rejuvenated secondary will appear brighter than the TAMS  $M_y$ . Assuming a minimum  $q = 0.3$  for the production of Be stars (Pols et al. 1991), we also identified the  $M_y$  of the mass gainer, shown as a dotted curve. (Note that for  $\log \text{age} > 7.5$ , the limiting  $M_y$  for the secondary is greater than  $y_{Bmax}$ .) Figure 8 reveals that only one of our definite Be stars is found at the TAMS and thus may have acquired its rapid rotation during a spin-up phase at this stage of its evolution. In contrast, we find that 38 Be stars, or 73%, fall in the mass range associated with binary mass ratios of  $0.3 \leq q < 1$  and are good candidates for spin-up by binary mass transfer. (Note that two Be stars in NGC 2439 have nearly the same  $M_y \approx -2.1$ , so these points overlap in Figure 8.) There are 14 Be stars below the binary mass ratio line of  $q < 0.3$ , and some of these were probably born as rapid rotators. However, four of these (members of the clusters NGC 6231, NGC 6322, and Stock 13) are likely Herbig Be stars, and their disks may be due either to rapid rotation or the remnants of star formation. We also caution that the  $M_y$  relations in Figure 8 neglect gravitational darkening and disk reddening in Be stars, so our comparison of the predictions of the three Be formation scenarios is not exact. Nevertheless, our results clearly emphasize the relative dominance of the binary spin-up process, while neither a TAMS spin-up phase nor

rapid rotation at the time of formation appear to play a significant role in the formation of Be stars.

We thank Charles Bailyn, Juan Zorec, and the referee, Helmut Abt, for their helpful comments on our manuscript. We are grateful to Charlie Finch and John Helsel for their help reducing the large amount of photometry. MVM thanks NOAO for travel support to observe with the CTIO 0.9m telescope, and she is supported by an NSF Astronomy and Astrophysics Postdoctoral Fellowship under award AST-0401460. Financial support also was provided by the NSF through grant AST-0205297 (DRG). Institutional support has been provided from the GSU College of Arts and Sciences and from the Research Program Enhancement fund of the Board of Regents of the University System of Georgia, administered through the GSU Office of the Vice President for Research.

Facilities: CTIO



## A. Notes on Individual Clusters

While the results from each cluster are summarized by Table 2, further comments regarding each cluster are presented below. The definite and possible Be stars in each cluster are identified using their assigned number from Table 1. (For cross referencing purposes, note that Table 1 lists other identifiers and WEBDA numbers for these stars whenever possible.) Particular sources of error, including saturated stars and contaminating foreground stars, are also discussed. Unless otherwise noted, spectral types and other information about individual stars are from the SIMBAD database.

The  $(b - y, y)$  color-magnitude and  $(b - y, y - H\alpha)$  color-color diagrams for each cluster are presented in Figures 9 – 63. In each color-magnitude diagram, the closest matching theoretical isochrone, assuming solar metallicity, from Lejeune & Schaerer (2001) is plotted as a solid line. The limiting magnitudes of B-type stars,  $y_{Bmin}$  and  $y_{Bmax}$ , are indicated as dashed lines when they are within the plotting range. In each color-color diagram, the theoretical color-color curve, derived from Kurucz (1979) model spectra, is shown as a solid line. Be stars are identified by their excess  $H\alpha$  brightness that shifts their  $y - H\alpha$  color above this reference line (Paper 1). We also made a parabolic fit of the color indices derived from dereddened spectra of 161 stars from the atlas of Jacoby, Hunter, & Christian (1984), shown as a dashed curve, and unreddened foreground stars will probably be found close to this curve in the observed color-color diagrams. In both diagrams, the massive O- and B-type stars all lie to the left of the vertical dashed line that represents  $E(b - y)$ . The definite and possible Be stars are represented with large diamonds in each plot, while all other stars are represented with small diamonds. In a few cases, potential foreground stars or white dwarfs that lie to the left of the reddening line have been excluded from the Be sample, and these stars are marked with an X.

- **Basel 1:** Only one star, GSC 05126 – 02385, is saturated in our images of Basel 1, and we detect no Be stars in this cluster.
- **Bochum 13:** Our images of Bochum 13 contain two bright, saturated stars: HD 156134 and HD 156154. The former is an O+ star, and the latter is a B0 Iab star. We identify Nos. 16 and 30 as definite Be stars, and No. 22 is a possible Be star candidate.

Aside from the two bright stars that are saturated, Bochum 13 is a sparse cluster that contains mostly fainter members. The MS is not well defined, and we find it difficult to determine accurate estimates of  $E(b - y)$ ,  $V_0 - M_V$ , and log age for this cluster. Therefore we consider our results less reliable, and we ignore this cluster in our statistics.

- **Collinder 272:** There are no saturated stars in our images of the cluster Collinder 272. The three Be stars in this cluster are Nos. 508, 565, and 767. We also find five possible Be stars: Nos. 345, 513, 560, 562, and 774.
- **Haffner 16:** In our images of Haffner 16, the cluster appears to have a small diameter of approximately  $4'$ , and many field stars are visible in the region. However, to create the color-magnitude and color-color diagrams of the cluster, we used the stars from the entire  $13'5 \times 13'5$  field of view of the CCD. From our color-magnitude diagram shown in Figure 12, the region of sky appears to contain two distinct stellar populations. Table 4 and Figure 1 reveal that Haffner 16 is located within the Perseus arm of the Galaxy and is viewed through the local spur, causing significant contamination from foreground stars along the line of sight.

Four stars in this cluster show  $H\alpha$  emission along with a color  $b - y < 0.123$ . One of the stars, No. 756, is within the dense cluster region and we classify it as a possible Be star. The others have a  $y$  magnitude fainter than the B star limit for the cluster, so they are likely foreground stars. There are three stars in our images of Haffner 16 that are saturated, but none are identified in the SIMBAD database.

- **Hogg 16:** Two stars are saturated in Hogg 16: HD 116887, a K0 III star, and HD 116875, a B8 V star. We find one possible Be star in Hogg 16, No. 195. The SIMBAD database also identifies No. 199 as a B2e star, and while we do observe  $H\alpha$  emission from this star, its  $b - y$  color is too red to classify it a B-type star in the cluster.

The cluster Hogg 16 lies about  $16'$  west of Collinder 272. We find slightly different  $E(b - y)$ ,  $V_0 - M_V$ , and ages for these two clusters, although they may be physically associated (Vázquez et al. 1997).

- **Hogg 22:** The only saturated star in our images of Hogg 22 is HD 150958, an O type star and a speckle binary with angular separation of  $0''.3$  (McAlister et al. 1990). We find one possible Be star, No. 9, in Hogg 22.

Hogg 22 is only  $6'$  away from the cluster NGC 6204. While the two appear almost as the same group on the sky, Hogg 22 is the more distant yet less evolved cluster (Forbes & Short 1996). Because the two clusters share the same FOV in our images, we used the finder chart of Forbes & Short (1996) to consider the photometry of Hogg 22 members separately. However, the known members of Hogg 22 do not include the full B-type MS, and as a result the cluster parameters have a large error. A more detailed analysis will be required to identify more cluster members.

- **IC 2395:** There are three saturated stars in our photometry of IC 2395: HD 74234, a B2 IV star; HD 74455, a B1.5 Vn star; and HD 74531, a B2 V star in a double system. We identify only one possible Be star candidate in this cluster, No. 92.

Our images of IC 2395 also contain members of the cluster BH 47, although both Clariá et al. (2003) and Jorgensen & Westerlund (1988) suggest that IC 2395 and BH 47 are really a single open cluster within the Vela OB1C association. Therefore we consider the entire field without discriminating between the two clusters.

- **IC 2581:** The very bright, saturated star that dominates images of this cluster is V399 Car, a Cepheid variable. Two other bright stars, HD 90706 and HD 90707, were defocused slightly during our observations to avoid saturation. HD 90706 is a B1/B2 Iab variable star (SIMBAD) and HD 90707 is a B1 III eclipsing binary (Lloyd Evans 1969).

Our photometry led to the detection of two definite Be stars in IC 2581. The first, No. 158, is a B2 Ve star, and the other is No. 243, a B1 Ve star. These two Be stars were also identified as Be stars by Lloyd Evans (1969, 1980). Lloyd Evans (1980) identifies No. 148 as a third Be star in IC 2581; however, it does not exhibit  $H\alpha$  emission in our results. We identify an additional 8 possible Be stars in IC 2581: Nos. 10, 123, 151, 157, 219, 267, 270, and 323.

- **IC 2944:** There are three saturated stars in our images of IC 2944. The first is HD 101131, an O6.5 V((f)) + O8.5 V spectroscopic binary (Gies et al. 2002). In addition, HD 101205 is an O8 star and eclipsing binary of  $\beta$  Lyr type, and HD 101298 is an O6 V star. We identify No. 58 as a definite Be star in IC 2944, and Nos. 21 and 51 are possible Be stars.

IC 2944 has a very distinctive appearance in our images; in addition to a slight amount of  $H\alpha$  nebulosity, several dark, sharp-edged Thackeray globules (Reipurth et al. 1997) are visible in the  $H\alpha$  images. Although these provide clear signs of active star formation in the field of IC 2944, there is disagreement within the literature about whether this is a significant physical cluster. While Walborn (1987) argues that the O stars of IC 2944 contribute to the ionization of an extensive HII region nearby, Perry & Landolt (1986) point out that both IC 2944 and IC 2948 are associated with this HII region in the Centaurus OB2 association, so the hot stars of IC 2944 are not required to ionize the region. They argue instead that IC 2944 is a chance superposition of early type field stars along the Carina arm of the Galaxy. Although the true nature of IC 2944 is not resolved, Figure 17 appears to represent a physically bound group, so we do include the cluster with our final statistics on Be stars in open clusters.

- **NGC 2343:** No stars are saturated in our images of NGC 2343, and we do not identify any Be stars in this cluster. Although Clariá (1972) identified our Nos. 19, 21, and 159 as probable foreground stars, they appear to lie on the cluster’s MS and we classify these stars as B-type stars within the cluster. Also, he found that our No. 160 is probably not a cluster member, although we find it close to the MS and barely too red to classify as another B star. Finally, Clariá (1972) identified No. 149 as a probable non-member of the cluster, but this star may be the only member of this sparse cluster to appear in the MS turnoff region, and confirmation of its membership in NGC 2343 could provide a better estimate of the cluster age.
- **NGC 2362:** Two stars in this cluster were saturated in our images, HD 57061 and HD 57192. HD 57061 is a quadruple star system containing a visual double, two O-type stars with a separation of  $0'.151$ . The brighter of the two O stars is a 154.9 day period spectroscopic binary that also contains an eclipsing binary with a 1.3 day period (van Leeuwen & van Genderen 1997). The other saturated star in our images of NGC 2362 is HD 57192, a B2 V eclipsing binary (Kazarovets et al. 1999). We do not identify any definite Be stars in this cluster, and there is only one star, No. 19, that we classify as a possible detection.
- **NGC 2367:** There are no definite Be stars in this cluster, and only three possible candidates: Nos. 55, 72, and 138. The two stars HD 57370 and BD  $-21^\circ 1881$  are saturated in our images of NGC 2367. HD 57370 is a B2/B3 III star, and BD  $-21^\circ 1881$  is a B1 V star. Although Ahumada & Lapasset (1995) classify HD 57370 as a blue straggler, we find several bright B-type stars in the cluster, and in fact NGC 2367 is one of the youngest clusters in this study.
- **NGC 2383:** Many of the stars in the nearby cluster NGC 2384 are in the same field of view as NGC 2383, so we removed the 13 known members of the neighboring cluster from this set of photometry. The only saturated star in our images of NGC 2383 is the star HD 58509, but because it is a member of NGC 2384, its photometry is included with that cluster’s data set. Two of the brightest stars in the field of NGC 2383 are not cluster members according to Subramaniam & Sagar (1999). They classify the first nonmember, No. 269, as an A3 I star. The other nonmember is No. 329, an M1 I star. Two definite Be stars are found in NGC 2383, Nos. 11 and 341.
- **NGC 2384:** Three known members of the nearby cluster NGC 2383 fell into the field of view of this cluster, so they were removed from the photometry set. None of the stars in NGC 2384 are saturated, and we found two possible Be stars in this cluster, Nos. 176 and 194.

Although the two clusters NGC 2383 and NGC 2384 are separated by only about  $5'$ , they are not associated. Vogt & Moffat (1972) and Subramaniam & Sagar (1999) have shown that NGC 2384 is both younger and at a farther distance than its neighbor, indicating a chance superposition in the plane of the Galaxy. According to Vogt & Moffat (1972), the two clusters have nearly the same reddening because NGC 2383 lies on the outer edge of the local spiral arm, so there is little dust between it and the more distant NGC 2384.

- **NGC 2414:** The star HD 60308, a B2 Iab star, is saturated in our images of NGC 2414. There are five definite Be stars in this cluster (Nos. 12, 65, 73, 87, and 97). In addition, we found 13 possible Be star candidates (Nos. 2, 3, 4, 14, 17, 19, 34, 37, 40, 106, 114, 119, and 122). However, there are a large number of apparent foreground stars contaminating the MS of this cluster, so we doubt that the Be candidates are true  $H\alpha$  emitters.

In fact, we doubt that this is a true, physically associated cluster. Although the group appears somewhat prominent against the field, we see two possible main-sequences in the color-magnitude diagram that we attempt to fit with different values for  $E(b - y)$  and  $V_0 - M_V$ . Neither value of  $E(b - y)$  provides a good match between the observed color-color sequence and the theoretical color-color curve, which suggests that the group either has a highly variable reddening or is not associated. We see no evidence for nebulosity or dust gradients in our  $H\alpha$  images of the cluster.

- **NGC 2421:** There are four stars in NGC 2421 with definite  $H\alpha$  emission and  $b - y < 0.350$ , the cutoff for OB stars based on the cluster’s reddening. These definite Be stars are Nos. 311, 356, 378, and 396. Slettebak (1985) observed  $H\gamma$  emission from No. 356 and classified its spectral type as B3–B5 (V:). He also observed weak  $H\gamma$  central emission in No. 311, which he also classified as a B3–B5 (V:) star. Also, Stephenson & Sanduleak (1977) identified No. 396 as a B9 star with weak emission lines. No. 378 is a newly identified Be star.

We also find six possible Be stars in NGC 2421: Nos. 83, 197, 256, 341, 483, and 530. Stephenson & Sanduleak (1977) also observed weak emission in No. 341. In addition, Stephenson & Sanduleak (1977) and Slettebak (1985) saw weak emission in No. 264, although this star is both too red and too faint in  $H\alpha$  to be a Be star in our results.

No stars in our images of NGC 2421 were saturated.

- **NGC 2439:** In our images of NGC 2439, there were two stars that had to be defocused to avoid saturation. The brightest is R Pup, an F8/G0 Ia star. Eggen (1983) describes R Pup as a “pseudo-cepheid”, a non-periodic variable supergiant whose low dispersion spectrum resembles a Cepheid. The second brightest star in the cluster is V384 Pup, an M3 Ia0-Ia pulsating variable star.

Our photometry of NGC 2439 revealed six definite Be stars, Nos. 22, 24, 58, 101, 193, and 196. No. 24 was classified as a B1 V: star with weak central emission in the  $H\gamma$  line by Slettebak (1985). He also observed double peaked  $H\alpha$  emission and sharp central absorption cores in the  $H\gamma$  and  $H\delta$  lines of No. 58. Slettebak (1985) also noted that the star No. 101 had been previously identified as a Be star, presumably in an unpublished catalog by Sanduleak & Robertson (1977). According to Slettebak, Sanduleak & Robertson list a total of five Be stars in NGC 2439, although the remaining two are not identified by Slettebak. In addition to the six definite Be stars found from our photometry, we detect seven possible cases: Nos. 13, 16, 43, 91, 116, 147, and 199.

NGC 2439 may not be a true open cluster (Eggen 1983; Kaltcheva, Gredel, & Fabricius 2001). Kaltcheva et al. (2001) found many localized clumps of OB stars within the cluster as well as highly variable reddening. In addition, they found a large scatter in distances, proper motions, and radial velocities among their sample of early type stars in the field. While NGC 2439 may simply be a collection of field stars revealed by an absorption hole in the galactic plane, its color-magnitude and color-color diagrams in Figure 25 appear to represent a true physical cluster, so we do include the cluster in our analysis in §3 and §4.

- **NGC 2483:** There were no stars that were saturated in our shortest exposures of this cluster, so there is no chance of any Be stars being overlooked. One of the definite Be stars in this cluster, No. 186, was classified as an A0 I emission line star by Stephenson & Sanduleak (1977), but they noted an uncertainty in the spectral type and a Be classification is likely. In addition, we identify No. 87 as a Be star, and there are ten possible Be stars in this cluster: Nos. 7, 27, 40, 42, 53, 90, 97, 179, 290, and 292.

NGC 2483 is not a true, physically associated cluster, and we ignore it in our analysis. FitzGerald & Moffat (1975) noted that the region has only a slight increase in the number density of stars over the background field, and they identified three distinct groups of stars, each at different distances, that are superimposed on the field. Havlen (1976) confirmed these results and recommended that NGC 2483 no longer be classified as a galactic cluster. Havlen also showed that the four bluest stars in our photometry are a group of foreground B6 – B8 stars that are somewhat less reddened (mean  $E(B - V) = 0.11$ ) than the population of 9 O9 – B5 stars that we used to fit the “cluster’s” isochrone.

- **NGC 2489:** There are no Be stars in this cluster, and no stars are saturated.
- **NGC 2571:** In our images of NGC 2571, no stars were saturated. The single Be star in this cluster is No. 76, and it is classified as a B4 star in SIMBAD.

- **NGC 2659:** None of the stars in NGC 2659 were saturated in our images. One definite Be star emerged from our color-color plot of this cluster, No. 233. In addition to this Be star, there are 4 possible Be stars (Nos. 3, 42, 89, and 222).
- **NGC 3293:** NGC 3293 is a young cluster with ongoing star formation around the cluster’s periphery (Baume et al. 2003), although its nuclear age is used in this study. Baume et al. found many pre-MS members in this cluster, as well as several massive stars that have already begun to move off of the ZAMS. Both they and Turner et al. (1980) observed variable reddening in this cluster, and our own H $\alpha$  image of NGC 3293 reveals thin, wispy clouds of gas across the region. The differential reddening is a likely cause for error in the isochrone fit, and the background H $\alpha$  emission as well as emission from pre-MS stars is also likely to contaminate the number of Be stars detected in this survey.

To further amplify the problem of detecting Be stars in NGC 3293, a large number of stars are saturated in our images of this bright cluster. They are: HD 91943, a B0.5/B1 II/III variable star; HD 91969, a B0 Ib star; HD 92007, a B1 III variable star of  $\lambda$  Eri type and a probable Be star (Balona 1994); HD 92044, a B1 II star; CD  $-57^{\circ}3348$ , a B0.5 V star; CPD  $-57^{\circ}3506B$ , a B1 III star that is a suspected eclipsing binary and a variable star of  $\beta$  Cep type (Balona 1994); CPD  $-57^{\circ}3521$ , a B1 III star; CPD  $-57^{\circ}3523$ , a B1 III star; CPD  $-57^{\circ}3526B$ , a B0.5 III star; and V361 Car, an M0 star. Clearly, the Be star population is probably not well sampled in this cluster due to the large number of B-type giants that are omitted from the photometry, including at least one probable Be star.

We find three definite Be stars in NGC 3293: Nos. 6, 42, and 46. In addition, there are eight possible Be stars with somewhat weaker emission: Nos. 4, 8, 27, 51, 54, 84, 99, and 116. No. 99 was noted to be a Be star by Shobbrook (1980), and No. 51 was also identified as a Be star by Feast (1958).

- **NGC 3766:** The cluster NGC 3766 was the test case for our photometric search for Be stars, and it was discussed in detail in Paper 1. The five definite Be stars that we identified with our photometry are (in our numbering scheme) Nos. 47, 127, 154, 198, and 200. Our spectra confirmed these five and also identified three other Be stars with weak H $\alpha$  emission: Nos. 31, 83, and 92. From our photometry, we classified Nos. 61, 73, 83, 92, 94, 126, 130, and 139 as possible Be detections. Our spectroscopy proves that at least some of these possible Be stars are indeed weak emission line stars.

The five saturated stars in our images of NGC 3766 are V910 Cen, HD 100840, HD 100943, HD 306794, and HD 306799. One of these saturated stars, HD 100943, was identified as a Be star by Shobbrook (1987) and confirmed by our spectra. However, for consistency in the detection technique, we only include Be stars detected with our photometry in this study.

- **NGC 4103:** No stars in our images of NGC 4103 were saturated. One star, No. 231, clearly exhibits H $\alpha$  emission in the color-color diagram of this cluster. It was classified as a B2 IVe star by Wesselink (1969), and we classify it as a definite Be star detection. Two other possible Be stars (Nos. 13 and 209) were also found in this cluster.
  - **NGC 4755:** In our images of NGC 4755, six bright stars are saturated. They are: HD 111904, a B9 Ia variable star; HD 111934, a B2 Ib variable star; HD 111973, a B5 Ia star; HD 111990, a B1/B2 Ib star in an optical double system; SAO 252073, an M2 Iab variable star of irregular type; and SAO 252075, a B0.5 Vn ellipsoidal variable star.
- Of the remaining unsaturated stars, five are definitely Be stars. They are: Nos. 43, 129 (B1.5 Vpne; Schild 1970), 171 (B2 IVne; Knoechel 1980), 180, and 187. Our photometry detected 7 additional Be star candidates (Nos. 20, 53, 131, 168, 189, 222, and 223).

- **NGC 5281:** One star, HD 119699, is saturated in our images of this cluster, and it is classified as an A1 II star. The only definite Be star detected in our study is No. 74, and five additional Be candidates were found: Nos. 11, 13, 29, 66, and 79. The bright star No. 80 also exhibits H $\alpha$  emission that distinguishes it in the color-color diagram, and it was previously classified as a Be star by Humphreys

(1975) and as a blue straggler by Ahumada & Lapasset (1995). However, its  $(b - y)$  color places it slightly redder than the B-type stars in our study so we do not classify it as a Be star, nor does it appear to be a blue straggler in the cluster.

- **NGC 5593:** There are no saturated stars in our images of NGC 5593. The star No. 204 is a definite Be star in this cluster, and No. 180 is a possible Be star.
- **NGC 6178:** The only saturated star in our images of NGC 6178 is HD 149277, a B2 IV/V star, and we do not identify any Be stars in this cluster.
- **NGC 6193:** This young cluster is rich in spectroscopic binaries, and Arnal et al. (1988) found a binary fraction as high as 72%. Two of the saturated stars in NGC 6193 are HD 150135 and HD 150136, an O6.5 V + O5 visual binary and the only two O stars in the Ara OB1 association (Herbst & Havlen 1977). In addition, the B1/B2 Ib supergiant HD 150041 is saturated in our images. NGC 6193 is an extremely young cluster, about the same age as the Orion nebula cluster (Herbst & Havlen 1977), with pre-MS B stars moving onto the ZAMS at magnitudes  $V > 12.4$  (Moffat & Vogt 1973). Therefore the possible Be star candidate in NGC 6193, No. 38, may be a pre-MS Herbig Be star.
- **NGC 6200:** Although the cluster NGC 6200 barely stands out against the background field, it contains a large number of B-type stars and Be star candidates. We identify Nos. 2, 38, 112, 213, 239, 247, 259, and 305 as possible Be stars and Nos. 115 and 153 as definite H $\alpha$  emission stars. NGC 6200 appears close to NGC 6204 and Hogg 22 on the sky, although this is a chance superposition since the cluster is younger and more distant than its apparent neighbors.
- **NGC 6204:** NGC 6204 is only 6' away from Hogg 22 on the sky (see the notes for that cluster). Members of Hogg 22 were removed from our results for NGC 6204, and no members of this cluster are saturated in our images. While we identify no definite Be stars in NGC 6204, there are two possible Be stars: Nos. 46 and 47. No. 4 was also identified as an H $\alpha$  emitter by Vega et al. (1980), but it is barely too red to be a B-type star according to our results.
- **NGC 6231:** NGC 6231 is a very bright cluster, and a large number of massive stars are saturated in our images. They are: HD 152233, an O6 III variable star; HD 152234, a B0.5 Ia star; HD 152248, an O7 I + O7 I spectroscopic binary (Penny, Gies, & Bagnuolo 1999); HD 152270 (WR 79), a WC+ Wolf-Rayet star; HD 326331, a B star; HD 152314, an O+ variable star; HD 152219, an O9 IV spectroscopic binary; SAO 227385, an O9 III spectroscopic binary; HD 152249, an O9 Ib supergiant; and HD 152218, an O9 V spectroscopic binary. The cluster has an extremely high binary frequency; Garca & Mermilliod (2001) found that 82% of the members earlier than B1.5 V are binary. It also contains a large number of pulsating variable stars, and Arentoft et al. (2001) identify at least 14 stars with  $\beta$  Cephei,  $\delta$  Scuti,  $\gamma$  Doradus, and other types of pulsations. We identify two definite Be stars, Nos. 67 and 79, and three possible Be stars, Nos. 2, 35, and 221, but none of these are identified as pulsators by Arentoft et al. (2001). Sung, Bessell, & Lee (1998) found 19 pre-MS stars or candidates in NGC 6231, including our Be star No. 79.
- **NGC 6249:** No stars are saturated in our images on NGC 6249, and we identify one definite Be star, No. 207.
- **NGC 6250:** There are two saturated stars in our images of NGC 6250. They are HD 152917, an A6 III/IV star, and HD 152853, a B2 III star. The cluster is sparse, with only seven B-type stars, and we find no Be stars in NGC 6250.
- **NGC 6268:** NGC 6268 is an evolved cluster with very few B stars remaining. We identify one of them, No. 51, as a definite Be star. The only saturated star in our images of this cluster is HD 322550, an F0 star and likely foreground to the cluster.

- **NGC 6322:** Three stars in NGC 6322 are saturated in our images, HD 156292, a B1 Ib/II supergiant, HD 156234, a B0 III star, and HD 156189, an A3 III/IV star. The definite Be star in this cluster is No. 12, and Nos. 7, 26, 50, 51, 76, 79, 84, and 85 are possible candidates. Most of these are likely Herbig Be stars as pre-MS contraction is still occurring in NGC 6322 among stars with  $V > 12.5$  (Moffat & Vogt 1975c).
- **NGC 6425:** The only saturated star in our images of NGC 6425 is HD 161508, a G6/G8 V star and likely a foreground star. We find no Be stars in this cluster.
- **NGC 6530:** NGC 6530 is part of a complex star-forming region, the Lagoon Nebula, and many of the bright B stars in the cluster are pre-MS stars moving onto the ZAMS (Sung, Chun, & Bessell 2000). The B0 IVpne star HD 164906 (Hiltner, Morgan, & Neff 1965) is saturated in our images of NGC 6530. We find one definite Be star, No. 50, and two possible Be stars, Nos. 20 and 31, in the cluster. No. 50 was classified as a B2 Ve star by Hiltner et al. (1965) and it was identified as a Herbig Be star by Boesono, The, & Tjin A Djie (1987).
- **NGC 6531:** The two stars HD 164863 and HD 164844 are saturated in our images of NGC 6531. They are O+ and B1/B2 III stars, respectively. Although Schild & Romanishin (1976) found no Be stars in this cluster, we see  $H\alpha$  emission from No. 12. Even though we classify this as a definite Be star because its  $y - H\alpha$  color is more than 5 standard deviations above the other B star colors, the photometry errors for this faint star are comparable to the strength of the emission so it may be a false Be star detection.
- **NGC 6604:** NGC 6604 appears faint without a well-defined MS in our images due to its location at the core of the HII region S54 (Barbon et al. 2000). The saturated star in our images is HD 167971, an O5–8 V + O5–8 V + O8 Ib triple system (Leitherer et al. 1987) and eclipsing binary of  $\beta$  Lyr type. The cluster may have some faint pre-MS members with  $V \geq 16$  (Barbon et al. 2000). There are seven possible Be stars in NGC 6604, Nos. 2, 3, 9, 11, 21, 66, and 73, although they all lie at the faint end of the MS and the errors in their  $y - H\alpha$  colors are relatively high. We believe that the apparent emission is more likely due to photometric scatter.
- **NGC 6613:** NGC 6613 = M18 is a sparse cluster in Sagittarius. No stars are saturated in our images of this cluster, and we find one definite Be star, No. 1, also discovered as an  $H\alpha$  emission star by MacConnell (1981).
- **NGC 6664:** No stars are saturated in our images of NGC 6664, and we find several Be star candidates. Nos. 177 and 221 have definite  $H\alpha$  emission, and Nos. 137 and 182 are possibly Be stars as well. Star No. 176 also appears to have  $H\alpha$  emission, but it is not classified as a B-type star in our results.
- **Ruprecht 79:** There is one star that is barely saturated in our  $b$  images of Ruprecht 79, but not much is known about it. The SIMBAD database identifies it as GSC 08585-01823 with  $B = 10.9$  and  $V = 10.28$ . Its color,  $B - V = 0.6$ , suggests that it is either a massive OB star in the cluster or an unreddened, foreground star. The latter is more likely, given the presence of many stars to the left of the MS which must be foreground stars. Walker (1987) points out that unreddened G and K stars fall into the same region as the reddened B and A stars in his color-color diagram of this cluster.

In a color-magnitude diagram of Ruprecht 79, the MS is not clearly defined due to the overlap of many foreground G and K stars (Walker 1987). They also contaminate the color-color plot, making it difficult to fit a theoretical reddening curve to our data. Because of the contamination, there are a large number of stars that lie more than  $2\sigma$  above the theoretical reddening curve in the Be star region of the color-color plot, but they are not likely to be Be stars since there is no clear gap in the stellar population indicating a group of  $H\alpha$  emitters. Therefore the Be star detections in this cluster are likely incorrect, and we disregard these detections in the analysis below.

The cluster Ruprecht 79 has been studied a handful of times in the literature (Moffat & Vogt 1975a; Harris & van den Bergh 1976; Walker 1987) because the Cepheid variable CS Velorum is a member of the cluster. However, Harris & van den Bergh (1976) note that the cluster is “rather loose”, and they point out that no large-scale photographs of the region were available at the time of their observing program. That is unfortunate, because a  $60' \times 60'$  image of Ruprecht 79 from the STScI Digitized Sky Survey reveals that Ruprecht 79 is not at all prominent against the field. In fact, the eastern half of the image is more crowded with stars than the west, suggesting a gradient in the dust absorption across the field. From our eyeball estimates, there are many other regions in the field with comparable stellar density to this cluster.

In addition, the galactic coordinates of Ruprecht 79 and its distance (see Table 4) place it within the Sagittarius-Carina spiral arm of the Milky Way (Binney & Merrifield 1998). The cluster is viewed through the tangential edge of the arm (Dame et al. 1987; Binney & Merrifield 1998), so a gradient in absorption across the field of view is likely. Therefore we conclude that Ruprecht 79 simply corresponds to a hole in the dust in this region of the Galaxy, and it is not a true open cluster.

- **Ruprecht 119:** Although Moffat & Vogt (1973) classified Ruprecht 119 as a non-cluster, Piatti et al. (2000b) showed that it is in fact physically bound. We find a distinct MS for the cluster, although we confirm a slight gap in the MS around  $y = 13.5$ , and possibly at  $y = 16$ , both identified by Piatti et al. (2000b). No stars are saturated in our results for Ruprecht 119, and we find one definite Be star (No. 332) and nine possible Be stars (Nos. 267, 301, 412, 427, 487, 549, 574, 674, and 706).
- **Ruprecht 127:** There are no saturated stars in our photometry of Ruprecht 127. We find no clear MS visible from our data, and any true MS is somewhat contaminated by field stars. We experimented with fitting the MS using the range of  $E(b-y)$ ,  $V_0 - M_V$ , and ages available in the literature (see Table 2) as well as our own values for a less reddened, closer group of stars. Each isochrone fit illustrated that multiple, sparse stellar populations are in the FOV, and there appear to be two stellar populations, with distinctly different reddening, in the color-color sequence as well. The Be star candidates found using the parameters in Table 2 are likely foreground stars rather than true emission stars. We find no Be stars when we fit the more nearby population. We doubt that this is a physical cluster, and instead we believe it is a chance physical alignment of several bright stars.
- **Ruprecht 140:** Only the star GSC 07397 – 00784 is saturated in our images of Ruprecht 140. We find no clear MS in this cluster, and we agree with Piatti & Clariá (2001) who concluded that Ruprecht 140 is not a physical cluster but rather a density fluctuation over the background field. We find one possible Be star in this FOV (No. 468).
- **Stock 13:** We find one definite Be star, No. 831, and one possible Be star, No. 271, in our results from Stock 13. No stars are saturated in our data. There may be some pre-MS stars in this cluster, as Moffat & Vogt (1975b) identified both Nos. 376 and 452 as possible pre-MS stars. We see a distinct cluster MS, although the color-color diagram possibly indicates a small population of nearly unreddened, late B- and early A-type foreground stars that are also present. Steppe (1977) also found a group of 20 foreground red giants in the field of Stock 13. The presence of foreground stars is not surprising considering the relatively large distance to this cluster (see Table 4).
- **Stock 14:** In our images of Stock 14, the F8 Ia supergiant V810 Cen is saturated, although Kienzle et al. (1998) found that this star is not a member of the cluster. We find one definite Be star (No. 164) and a possible Be star (No. 105) in Stock 14, and both of these stars are also identified as Be or emission line stars in SIMBAD.
- **Trumpler 7:** No definite Be stars are found in this cluster, but 5 possible Be stars have  $H\alpha$  emission more than  $2\sigma$  above the color-color fit. These Be star candidates are Nos. 13, 55, 57, 59, and 82. Only the A1 IV star HD 59163 is saturated in our images of Trumpler 7.



- **Trumpler 18:** No stars are saturated in our results from Trumpler 18, and we identify five possible Be stars (Nos. 10, 29, 55, 137, and 219). Like Vázquez & Feinstein (1990), we see a clear MS for this cluster. However, Vázquez & Feinstein (1990) questioned the physical association of Trumpler 18 because they found a peculiar luminosity function for the cluster. We compute the mass function for Trumpler 18 based on the method described in §3, and we find a normal power law relation with  $\Gamma = -1.5 \pm 0.16$ , depending on the number of  $\log M$  bins used. With this value of  $\Gamma$  we should expect  $75 \pm 4$  B-type stars in the cluster, and we detect 71 (see Table 2). We conclude that Trumpler 18 is a true open cluster.
- **Trumpler 20:** There are no saturated stars in our images of Trumpler 20. We find very few B-type stars in this cluster, and only one possible Be star (No. 1039).
- **Trumpler 27:** We find two saturated stars in our images of Trumpler 27: HD 318014, a B8 Iab supergiant, and CD  $-33^{\circ}12241$ , an M0 Ia binary. The cluster contains one star with very strong emission, No. 15 (WR 95). In this case, the emission more likely originates from the He II  $\lambda$  6527 line than H $\alpha$  in this Wolf-Rayet star. We also find two possible Be stars, Nos. 49 and 52. We do not see a well defined MS for Trumpler 27, although we believe this is due to the cluster’s significant differential reddening. Thé & Stokes (1970) found that the cluster lies behind the dust lane B217 that partially encircles the cluster, and Feinstein et al. (2000) used polarization measurements to determine that two separate dust components lie in the field of Trumpler 27. We believe that our estimates of the cluster parameters are unreliable, and we disregard this cluster in our statistical analysis of Be stars (§3).
- **Trumpler 28:** The B3 star HD 317971 is saturated in our images of Trumpler 28, and we find no Be stars in this cluster.

The cluster Trumpler 28 is only  $14'$  from NGC 6383, and the two may form a binary open cluster system (Subramaniam et al. 1995). However, the large angular size of NGC 6383 ( $20'$ ; WEBDA) excluded it from our target list, and we do not present photometry of that cluster in this study. According to Subramaniam et al. (1995), NGC 6383 is significantly younger than Trumpler 28, and the three apparent blue stragglers near the MS of Trumpler 28 (Nos. 139, 161, and 193) are probably members of NGC 6383 instead.

- **Trumpler 34:** No stars are saturated in our images of Trumpler 34. We find one definite Be star, No. 355, and one possible Be star, No. 297, in this cluster. No. 355 is very blue for a late B-type star, but its photometric errors are small enough that we trust its position in Figure 62. However, it may possibly be a foreground star.
- **vdB-Hagen 217:** There are no saturated stars in our images of vdB-Hagen 217. We find no Be stars in this cluster.

## REFERENCES

- Abt, H. A. 1979, *ApJ*, 230, 485
- Abt, H. A. 1987, in *Physics of Be Stars*, ed. A. Slettebak & T. P. Snow (Cambridge: Cambridge Univ. Press), 470
- Abt, H. A., Levato, H., & Grosso, M. 2002, *ApJ*, 573, 359
- Abt, H. A., & Levy, S. G. 1978, *ApJS*, 36, 241
- Ahumada, A. V., Clariá, J. J., Bica, E., & Piatti, A. E. 2000, *A&AS*, 141, 79
- Ahumada, J., & Lapasset, E. 1995, *A&AS*, 109, 375
- Alfaro, E. J., & Delgado, A. J. 1991, *A&A*, 241, 69
- Arentoft, T., Sterken, C., Knudsen, M. R., Freyhammer, L. M., Duerbeck, H. W., Pompei, E., Delahodde, C. E., & Clasen, J. W. 2001, *A&A*, 380, 599
- Arnal, M., Morrell, N., Garcia, B., & Levato, H. 1988, *PASP*, 100, 1076
- Babu, G. S. D. 1983, *J. Astrophys. Astr.*, 4, 235
- Balona, L. A. 1994, *MNRAS*, 267, 1060
- Barai, P., et al. 2004, *ApJ*, 608, 989
- Barbon, R., Carraro, G., Munari, U., Zwitter, T., & Tomasella, L. 2000, *A&AS*, 144, 451
- Baume, G., Vázquez, R. A., Carraro, G., & Feinstein, A. 2003, *A&A*, 402, 549
- Binney, J., & Merrifield, M. 1998, *Galactic Astronomy* (Princeton: Princeton Univ. Press)
- Bissantz, N., Englmaier, P., & Gerhard, O. 2003, *MNRAS*, 340, 949
- Boesono, B., The, P. S., & Tjin A Djie, H. R. E. 1987, *Ap&SS*, 137, 167
- Carraro, G., & Munari, U. 2004, *MNRAS*, 347, 625
- Clariá, J. J. 1972, *AJ*, 77, 868
- Clariá, J. J., Lapasset, E., Piatti, A. E., & Ahumada, A. V. 2003, *A&A*, 409, 541
- Clausen, J. V., Larsen, S. S., Garcia, J. M., Giménez, A., & Storm, J. 1997, *A&AS*, 122, 559
- Cordes, J. M., & Lazio, T. J. W. 2003, *astro-ph/0207156*
- Cousins, A. W. J. 1987, *South African Astron. Obs. Circ.*, 11, 93
- Cousins, A. W. J., & Caldwell, J. A. R. 1985, *Obs.*, 105, 134
- Dame, T. M., et al. 1987, *ApJ*, 322, 706
- Delgado, A. J., Alfaro, E. J., & Cabrera-Cano, J. 1997, *AJ*, 113, 713
- Eggen, O. J. 1983, *AJ*, 88, 386
- Fabregat, J., & Torrejón, J. M. 2000, *A&A*, 357, 451
- Feast, M. W. 1958, *MNRAS*, 118, 618
- Feinstein, C., Baume, G., Vazquez, R., Niemela, V., & Cerruti, M. A. 2000, *AJ*, 120, 1906
- FitzGerald, M. P., Luiken, M., Maitzen, H. M., & Moffat, A. F. J. 1979, *A&AS*, 37, 345
- FitzGerald, M. P., & Moffat, A. F. J. 1975, *A&AS*, 20, 289
- Fitzpatrick, E. L. 1999, *PASP*, 111, 63
- Forbes, D., & Short, S. 1996, *AJ*, 111, 1609
- Frémat, Y., Zorec, J., Hubert, A.-M., & Floquet, M. 2005, *A&A*, in press (*astro-ph/0503381*)
- García, B., & Mermillod, J. C. 2001, *A&A*, 368, 122
- Gies, D. R. 2000, *ASP Conf. Ser.* 214: *IAU Colloq. 175: The Be Phenomenon in Early-Type Stars*, 214, 668
- Gies, D. R., Bagnuolo, W. G., Jr., Ferrara, E. C., Kaye, A. B., Thaller, M. L., Penny, L. R., & Peters, G. J. 1998, *ApJ*, 493, 440
- Gies, D. R., Penny, L. R., Mayer, P., Drechsel, H., & Lorenz, R. 2002, *ApJ*, 574, 957
- Grebel, E. K. 1997, *A&A*, 317, 448

- Hagen, G. L. 1970, Publications of the David Dunlap Observatory, 4, 1
- Harmanec, P. 1988, Bulletin of the Astronomical Institutes of Czechoslovakia, 39, 329
- Harris, G. L. H., & van den Bergh, S. 1976, ApJ, 209, 130
- Havlen, R. J. 1976, A&A, 50, 227
- Herbst, W., & Havlen, R. J. 1977, A&AS, 30, 279
- Hilditch, R. W. 2001, An Introduction to Close Binary Stars (Cambridge: Cambridge Univ. Press)
- Hiltner, W. A., Morgan, W. W., & Neff, J. S. 1965, ApJ, 141, 183
- Hoffleit, D., & Warren, W. H., Jr. 1991, Bright Star Catalogue, 5th Revised Ed. (New Haven: Yale Univ. Obs.)
- Humphreys, R. M. 1975, A&AS, 19, 243
- Jacoby, G. H., Hunter, D. A., & Christian, C. A. 1984, ApJS, 56, 257
- Jorgensen, U. G., & Westerlund, B. E. 1988, A&AS, 72, 193
- Kaltcheva, N., Gredel, R., & Fabricius, C. 2001, A&A, 372, 95
- Kalirai, J. S., et al. 2001, AJ, 122, 257
- Kazarovets, A. V., Samus, N. N., Durlevich, O. V., Frolov, M. S., Antipin, S. V., Kireeva, N. N., & Pastukhova, E. N. 1999, Information Bulletin on Variable Stars, 4659, 1
- Keller, S. C., Grebel, E. K., Miller, G. J., & Yoss, K. M. 2001, AJ, 122, 248
- Keller, S. C., Wood, P. R., & Bessell, M. S. 1999, A&AS, 134, 489
- Kienzle, F., Burki, G., Burnet, M., & Meynet, G. 1998, A&A, 337, 779
- Knoechel, G. 1980, A&A, 82, 253
- Kurucz, R. L. 1979, ApJS, 40, 1
- Leitherer, C., et al. 1987, A&A, 185, 121
- Lejeune, T., & Schaerer, D. 2001, A&A, 366, 538
- Lindoff, U. 1971, A&A, 15, 439
- Lloyd Evans, T. 1969, MNRAS, 146, 101
- Lloyd Evans, T. 1980, MNRAS, 192, 47
- Lynga, G. 1987, Catalogue of Open Cluster Data (5th Ed.), Lund Obs. Publ., online at Vizier no. VII/92A
- MacConnell, D. J. 1981, A&AS, 44, 387
- Maeder, A., Grebel, E. K., & Mermilliod, J.-C. 1999, A&A, 346, 459
- Maintz, M., Rivinius, T., Stahl, O., Štefl, S., & Appenzeller, I. 2004, Astronomische Nachrichten Supplement, 325, 18
- Massey, P., Johnson, K. E., & Degioia-Eastwood, K. 1995, ApJ, 454, 151
- McAlister, H., Hartkopf, W. I., & Franz, O. G. 1990, AJ, 99, 965
- McSwain, M. V., & Gies, D. R. 2005, ApJ, 622, 1052 (Paper 1)
- Mermilliod, J.-C. 1982, A&A, 109, 48
- Meynet, G., & Maeder, A. 2000, A&A, 361, 101
- Moffat, A. F. J., & Vogt, N. 1973, A&AS, 10, 135
- Moffat, A. F. J., & Vogt, N. 1975a, A&AS, 20, 85
- Moffat, A. F. J. & Vogt, N. 1975b, A&AS, 20, 125
- Moffat, A. F. J., & Vogt, N. 1975c, A&AS, 20, 155
- Paunzen, E., & Maitzen, H. M. 2001, A&A, 373, 153
- Penny, L. R., Gies, D. R., & Bagnuolo, W. G., Jr. 1999, ApJ, 518, 450
- Perrot, C. A., & Grenier, I. A. 2003, A&A, 404, 519
- Perry, C. L., Hill, G., & Christodoulou, D. M. 1991, A&AS, 90, 195
- Perry, C. L., & Landolt, A. U. 1986, AJ, 92, 844
- Piatti, A. E., Bica, E., & Clariá, J. J. 2000b, A&A, 362, 959
- Piatti, A. E., & Clariá, J. J. 2001, A&A, 370, 931

- Piatti, A. E., Clariá, J. J., & Bica, E. 2000a, *A&A*, 360, 529
- Pols, O. R., Coté, J., Waters, L. B. F. M., & Heise, J. 1991, *A&A*, 241, 419
- Porter, J. M., & Rivinius, T. 2003, *PASP*, 115, 1153
- Raguzova, N. V., & Popov, S. B. 2005, *MNRAS*, in press (astro-ph/0505275)
- Reipurth, B., Corporon, P., Olberg, M., & Tenorio-Tagle, G. 1997, *A&A*, 327, 1185
- Rivinius, T., Štefl, S., Maintz, M., Stahl, O., & Baade, D. 2004, *A&A*, 427, 307
- Sanner, J., Brunzendorf, J., Will, J.-M., & Geffert, M. 2001, *A&A*, 369, 511
- Schild, R. E. 1970, *ApJ*, 161, 855
- Schild, R., & Romanishin, W. 1976, *ApJ*, 204, 493
- Schlegel, D. J., Finkbeiner, D. P., & Davis, M. 1998, *ApJ*, 500, 525
- Schmidt, E. G. 1982, *AJ*, 87, 1197
- Shobbrook, R. R. 1980, *MNRAS*, 192, 821
- Shobbrook, R. R. 1985, *MNRAS*, 212, 591
- Shobbrook, R. R. 1987, *MNRAS*, 225, 999
- Slettebak, A. 1949, *ApJ*, 110, 498
- Slettebak, A. 1966, *ApJ*, 145, 126
- Slettebak, A. 1985, *ApJS*, 59, 769
- Slettebak, A., Collins, G. W., II, & Truax, R. 1992, *ApJS*, 81, 335
- Steppe, H. 1977, *A&AS*, 27, 415
- Stetson, P. B. 1981, *AJ*, 86, 1500
- Stephenson, C. B., & Sanduleak, N. 1977, *ApJS*, 33, 459
- Strom, S. E., Wolff, S. C., & Dror, D. 2005, *AJ*, 129, 809
- Subramaniam, A., Gorti, U., Sagar, R., & Bhatt, H. C. 1995, *A&A*, 302, 86
- Subramaniam, A., & Sagar, R. 1999, *AJ*, 117, 937
- Sung, H., Bessell, M. S., & Lee, S. 1998, *AJ*, 115, 734
- Sung, H., Chun, M., & Bessell, M. S. 2000, *AJ*, 120, 333
- Tadross, A. L. 2001, *New Astronomy*, 6, 293
- Thaller, M. L., Bagnuolo, W. G., Jr., Gies, D. R., & Penny, L. R. 1995, *ApJ*, 448, 878
- Thé, P. S., & Stokes, N. 1970, *A&A*, 5, 298
- Townsend, R. H. D., Owocki, S. P., & Howarth, I. D. 2004, *MNRAS*, 350, 189
- Turner, D. G. 1990, *PASP*, 102, 1331
- Turner, D. G., Grieve, G. R., Herbst, W., & Harris, W. E. 1980, *AJ*, 85, 1193
- Van Bever, J., & Vanbeveren, D. 1997, *A&A*, 322, 116
- van Leeuwen, F., & van Genderen, A. M. 1997, *A&A*, 327, 1070
- Vázquez, R. A., Baume, G., Feinstein, A., & Prado, P. 1997, *A&AS*, 124, 13
- Vázquez, R. A., & Feinstein, A. 1990, *A&AS*, 86, 209
- Vega, E. I., Rabolli, M., Feinstein, A., & Muzzio, J. C. 1980, *AJ*, 85, 1207
- Vogt, N., & Moffat, A. F. J. 1972, *A&AS*, 7, 133
- Walborn, N. R. 1987, *AJ*, 93, 868
- Walker, A. R. 1987, *MNRAS*, 229, 31
- Waters, L. B. F. M., Cote, J., & Pols, O. R. 1991, *A&A*, 250, 437
- Wesselink, A. J. 1969, *MNRAS*, 146, 329
- Zorec, J., & Briot, D. 1997, *A&A*, 318, 443

---

This 2-column preprint was prepared with the AAS L<sup>A</sup>T<sub>E</sub>X macros v5.2.

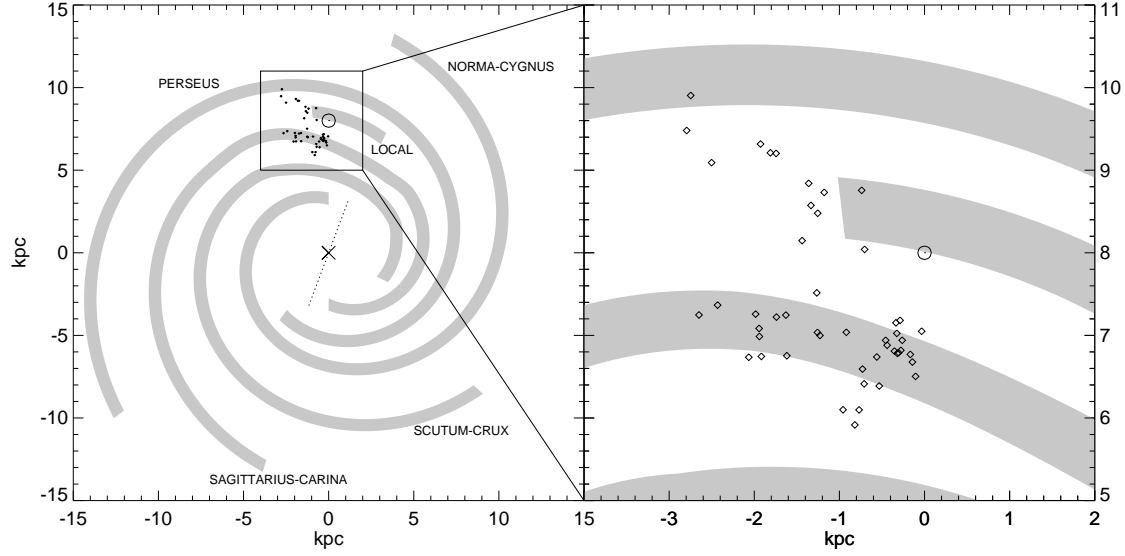


Fig. 1.— The distribution of the true open clusters is shown relative to the Sun ( $\odot$ ) and the Galactic center ( $\times$ ). The positions of the spiral arms (*gray*) are from Cordes & Lazio (2003), and the orientation of the central bar (*dotted line*) is from Bissantz, Englmaier, & Gerhard (2003).

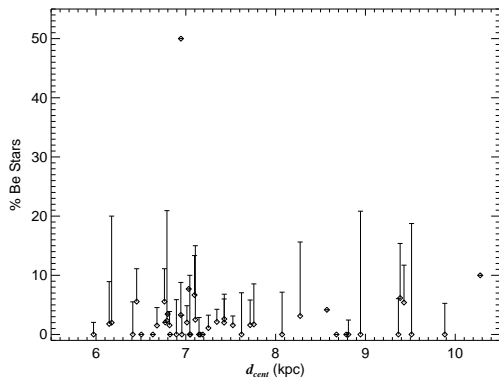


Fig. 2.— The percentage of Be stars (*diamonds*) is shown as a function of their distance from the Galactic center,  $d_{cent}$ . The upper limit for each cluster, the percentage of definite and possible Be stars, is also shown.

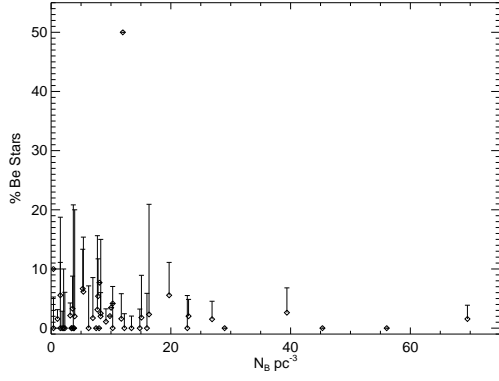


Fig. 3.— The percentage of Be stars is shown as a function of the cluster density in the same format as Figure 2.

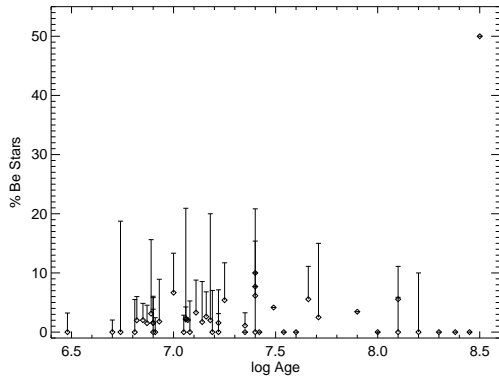


Fig. 4.— The percentage of definite Be stars is shown as a function of cluster age in the same format as Figure 2.

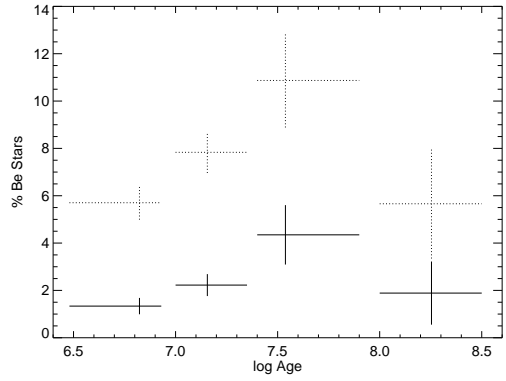


Fig. 5.— The average definite Be frequency (*solid lines*) and total possible Be frequency (*dashed lines*) are plotted for four age bins corresponding to  $\log \text{age} < 7.0$ ,  $7.0 \leq \log \text{age} < 7.4$ ,  $7.4 \leq \log \text{age} < 8.0$ , and  $\log \text{age} \geq 8.0$ . The errors in Be frequency represent the Poisson statistics for our sample, and the age error bars represent the maximum and minimum ages observed in each bin.

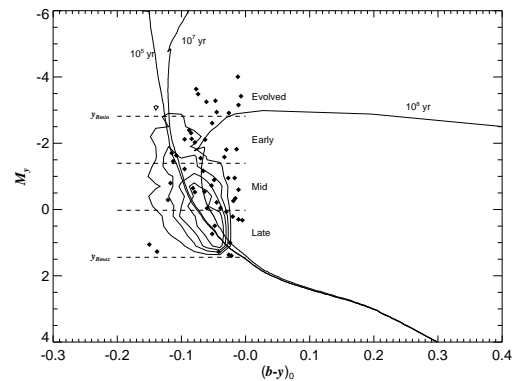


Fig. 6.— The definite Be star detections are shown on an absolute color-magnitude diagram. Three isochrones with ages  $10^5$ ,  $10^7$ , and  $10^8$  yr are shown for comparison. The B stars are divided into four regions: evolved, early, mid, and late spectral types. The contours represent the distribution of normal B-type stars detected in our sample (29%, 43%, 57%, and 76%, respectively).

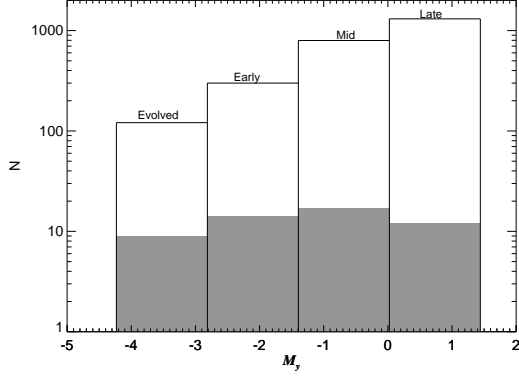


Fig. 7.— A histogram plot of the total Be and B star populations of all clusters. The bins are divided into evolved, early, mid, and late B spectral types.

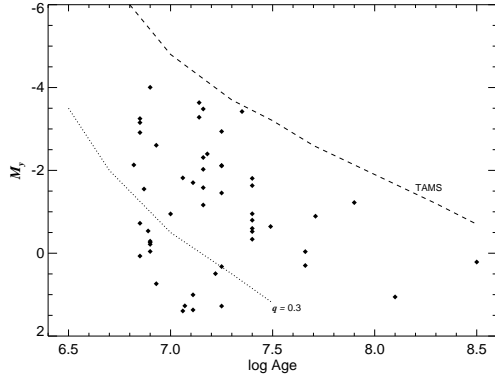


Fig. 8.—  $M_y$  of the definite Be stars is plotted as a function of cluster age (*diamonds*). The absolute magnitude of a B star at the TAMS is also shown (*dashed curve*; Lejeune & Schaerer 2001). For a primary at the TAMS and system mass ratio  $q = 0.3$ ,  $M_y$  of the secondary is also shown (*dotted curve*).

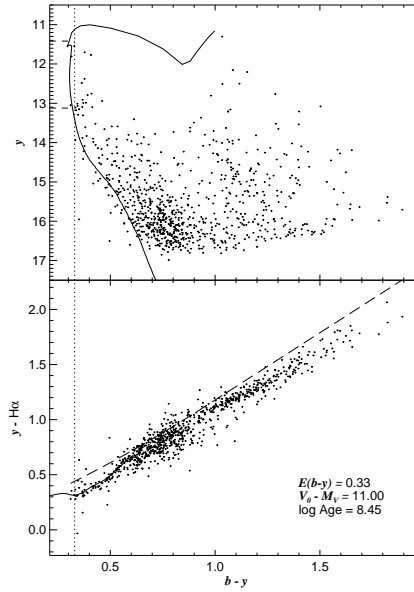


Fig. 9.— Color-magnitude (*top*) and color-color (*bottom*) diagrams of the cluster Basel 1. The isochrone fit (*solid line in top*), color-color fit (*solid line in bottom*), reddening value (*dotted lines*),  $y_{Bmin}$  and  $y_{Bmax}$  (*dashed lines in top*), and parabolic fit of unreddened stars in the atlas of Jacoby et al. (1984) (*dashed line in bottom*) are also shown. Be stars (*large*) are distinguished from all other stars (*small*) in both diagrams (although in this cluster no Be stars are present). Potential foreground stars or white dwarfs are also marked ( $\times$ ), although none are present in our data for this cluster.

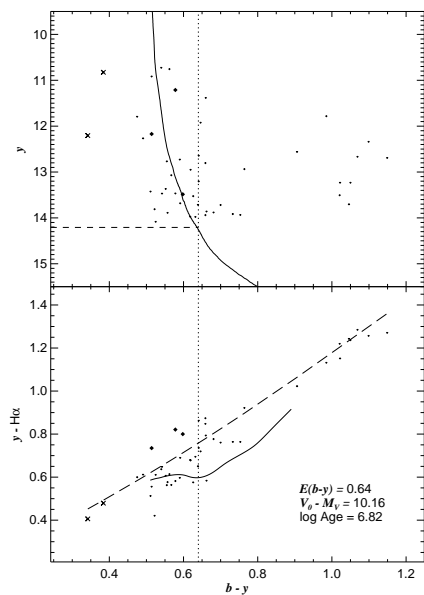


Fig. 10.— Color-magnitude (*top*) and color-color (*bottom*) diagrams of the cluster Bochum 13 in the same format as Figure 9.

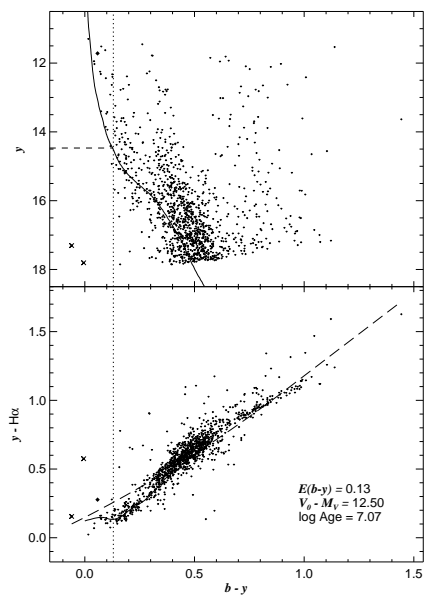


Fig. 12.— Color-magnitude (*top*) and color-color (*bottom*) diagrams of the cluster Haffner 16 in the same format as Figure 9.

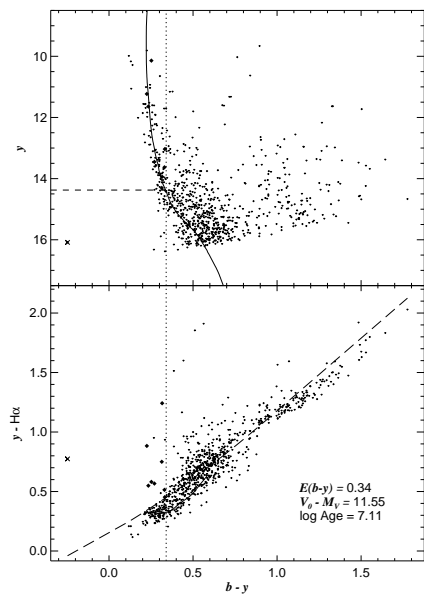


Fig. 11.— Color-magnitude (*top*) and color-color (*bottom*) diagrams of the cluster Collinder 272 in the same format as Figure 9.

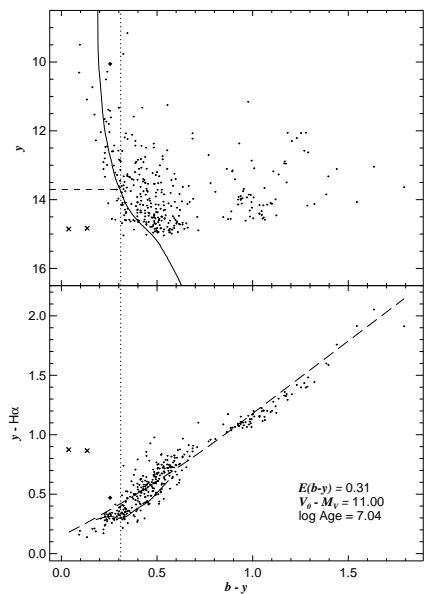


Fig. 13.— Color-magnitude (*top*) and color-color (*bottom*) diagrams of the cluster Hogg 16 in the same format as Figure 9.



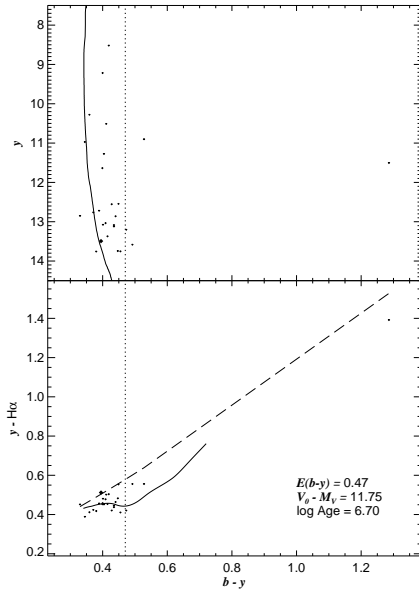


Fig. 14.— Color-magnitude (*top*) and color-color (*bottom*) diagrams of the cluster Hogg 22 in the same format as Figure 9.

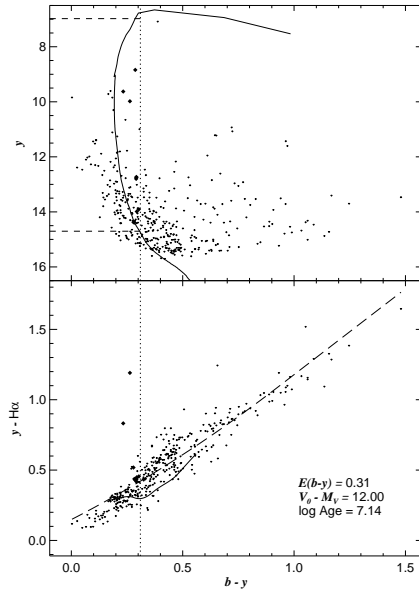


Fig. 16.— Color-magnitude (*top*) and color-color (*bottom*) diagrams of the cluster IC 2581 in the same format as Figure 9.

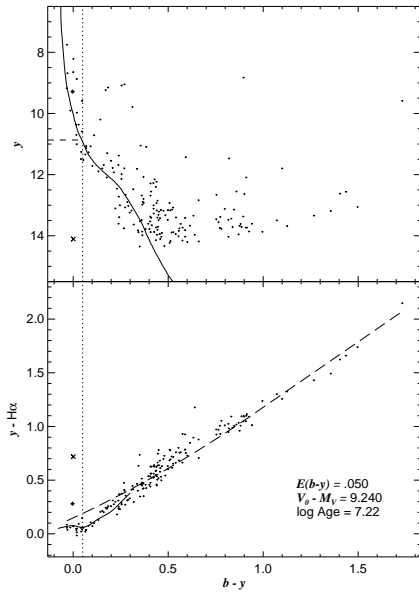


Fig. 15.— Color-magnitude (*top*) and color-color (*bottom*) diagrams of the cluster IC 2395 in the same format as Figure 9.

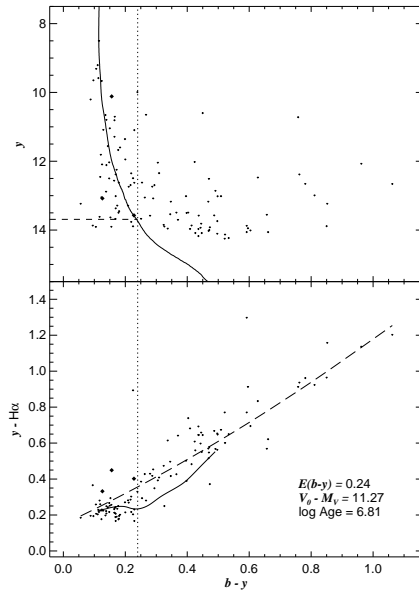


Fig. 17.— Color-magnitude (*top*) and color-color (*bottom*) diagrams of the cluster IC 2944 in the same format as Figure 9.

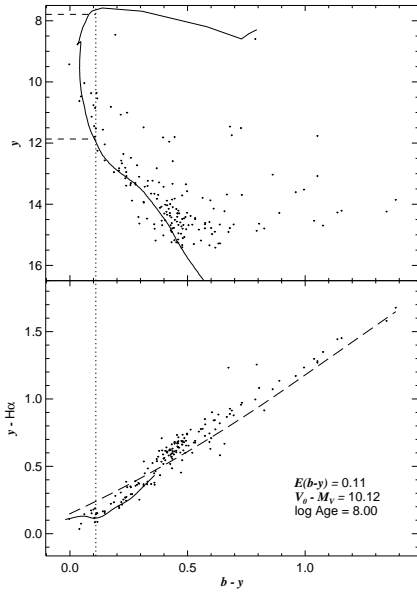


Fig. 18.— Color-magnitude (*top*) and color-color (*bottom*) diagrams of the cluster NGC 2343 in the same format as Figure 9.

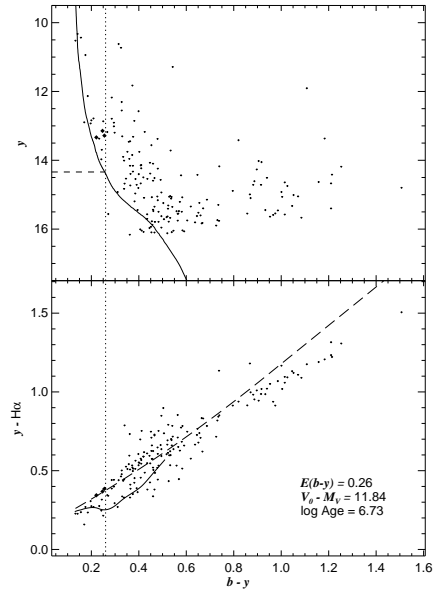


Fig. 20.— Color-magnitude (*top*) and color-color (*bottom*) diagrams of the cluster NGC 2367 in the same format as Figure 9.

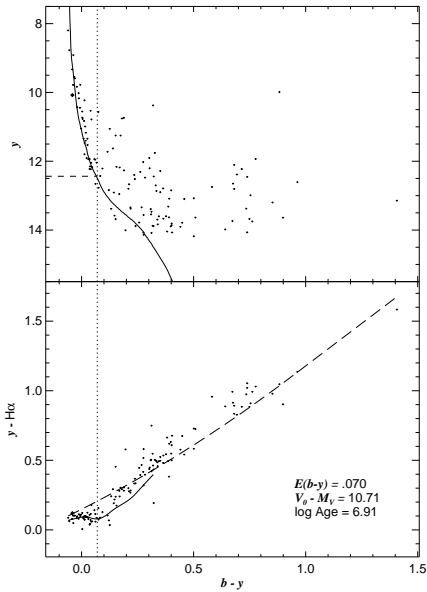


Fig. 19.— Color-magnitude (*top*) and color-color (*bottom*) diagrams of the cluster NGC 2362 in the same format as Figure 9.

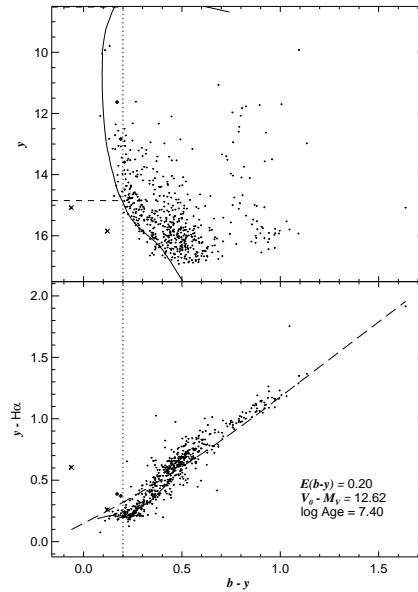


Fig. 21.— Color-magnitude (*top*) and color-color (*bottom*) diagrams of the cluster NGC 2383 in the same format as Figure 9.

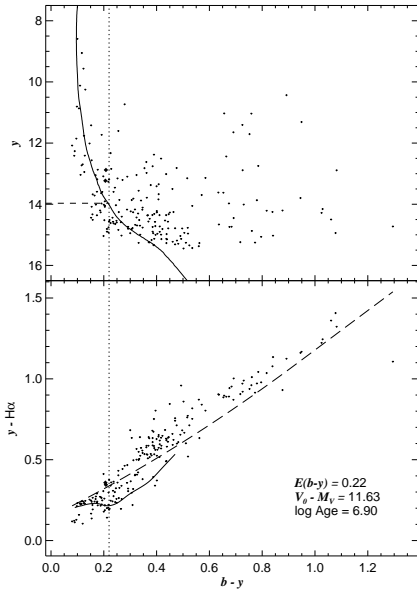


Fig. 22.— Color-magnitude (*top*) and color-color (*bottom*) diagrams of the cluster NGC 2384 in the same format as Figure 9.

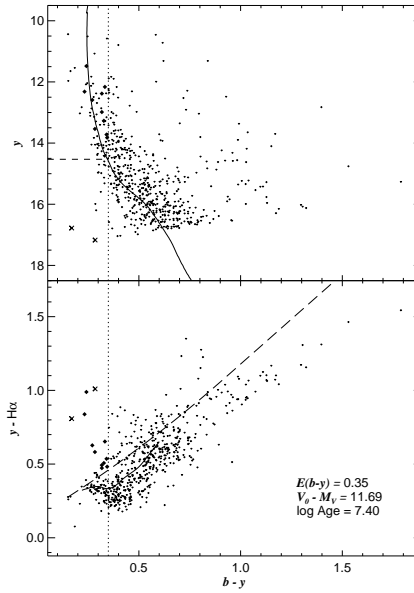


Fig. 24.— Color-magnitude (*top*) and color-color (*bottom*) diagrams of the cluster NGC 2421 in the same format as Figure 9.

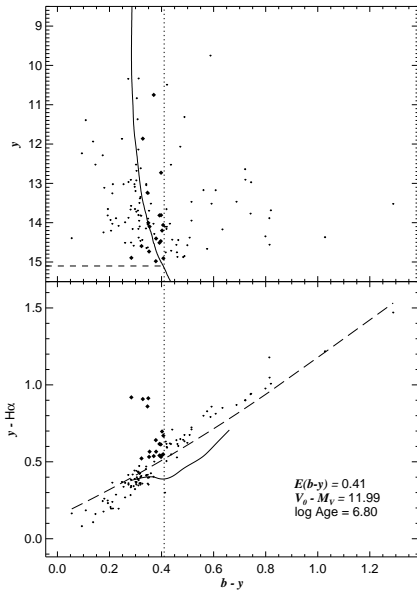


Fig. 23.— Color-magnitude (*top*) and color-color (*bottom*) diagrams of the cluster NGC 2414 in the same format as Figure 9.

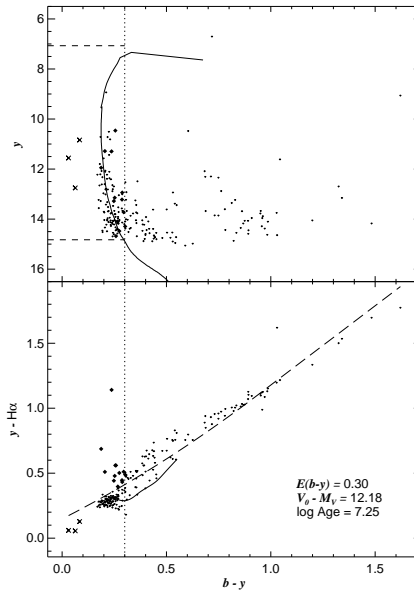


Fig. 25.— Color-magnitude (*top*) and color-color (*bottom*) diagrams of the cluster NGC 2439 in the same format as Figure 9.

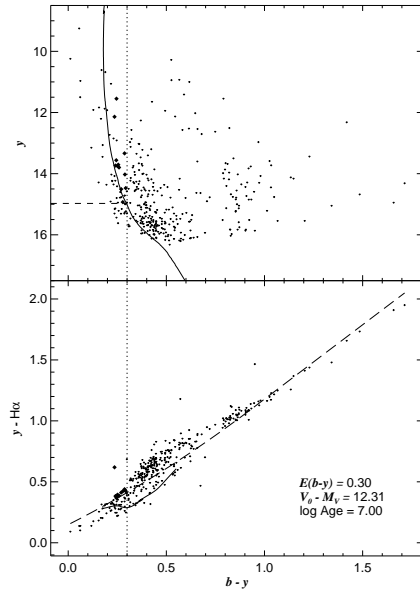


Fig. 26.— Color-magnitude (*top*) and color-color (*bottom*) diagrams of the cluster NGC 2483 in the same format as Figure 9.

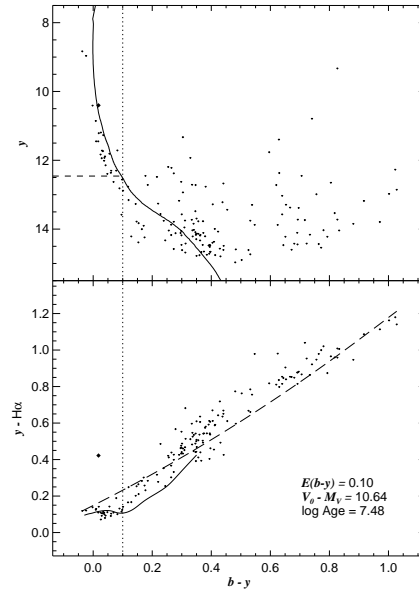


Fig. 28.— Color-magnitude (*top*) and color-color (*bottom*) diagrams of the cluster NGC 2571 in the same format as Figure 9.

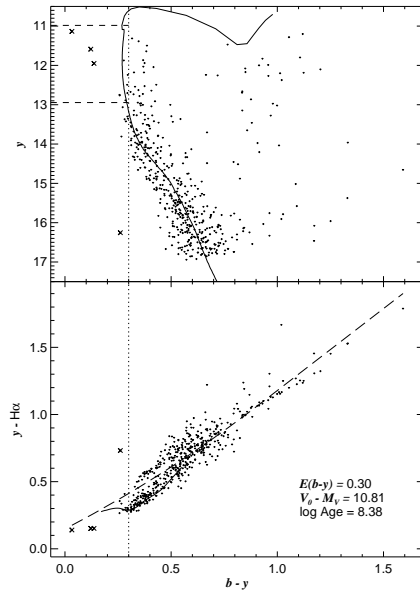


Fig. 27.— Color-magnitude (*top*) and color-color (*bottom*) diagrams of the cluster NGC 2489 in the same format as Figure 9.

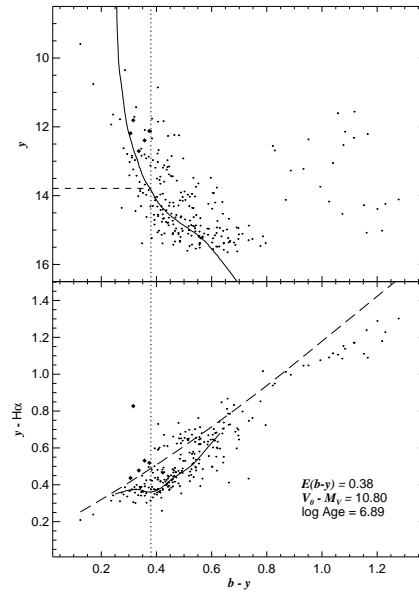


Fig. 29.— Color-magnitude (*top*) and color-color (*bottom*) diagrams of the cluster NGC 2659 in the same format as Figure 9.

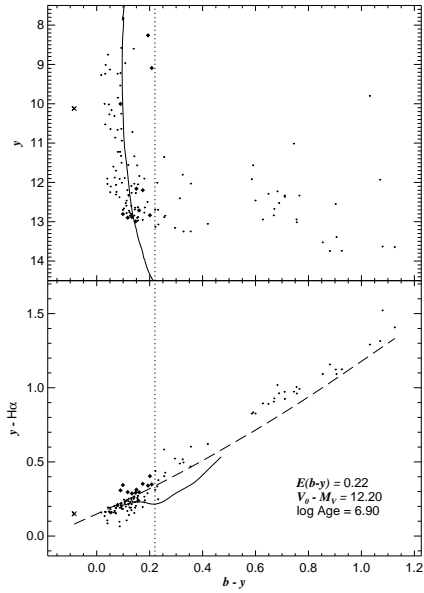


Fig. 30.— Color-magnitude (*top*) and color-color (*bottom*) diagrams of the cluster NGC 3293 in the same format as Figure 9.

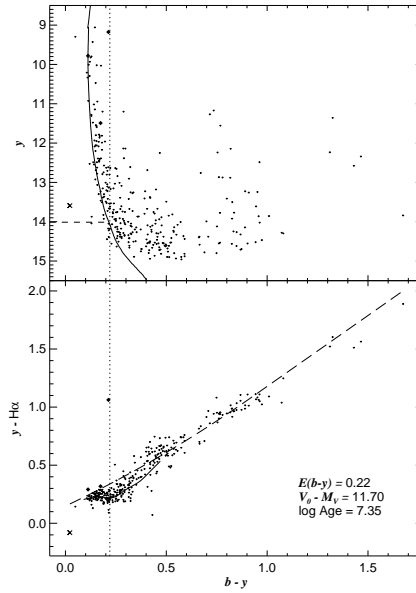


Fig. 32.— Color-magnitude (*top*) and color-color (*bottom*) diagrams of the cluster NGC 4103 in the same format as Figure 9.

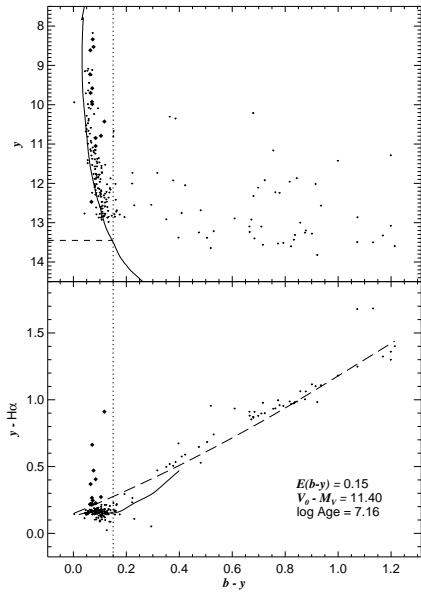


Fig. 31.— Color-magnitude (*top*) and color-color (*bottom*) diagrams of the cluster NGC 3766 in the same format as Figure 9.

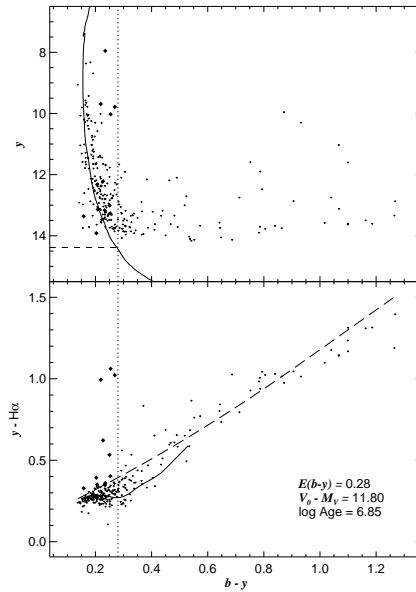


Fig. 33.— Color-magnitude (*top*) and color-color (*bottom*) diagrams of the cluster NGC 4755 in the same format as Figure 9.

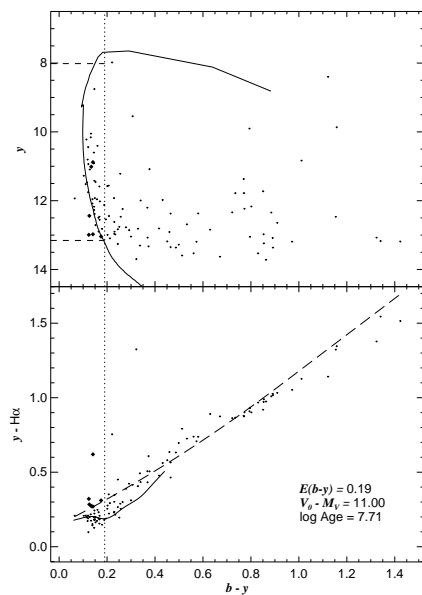


Fig. 34.— Color-magnitude (*top*) and color-color (*bottom*) diagrams of the cluster NGC 5281 in the same format as Figure 9.

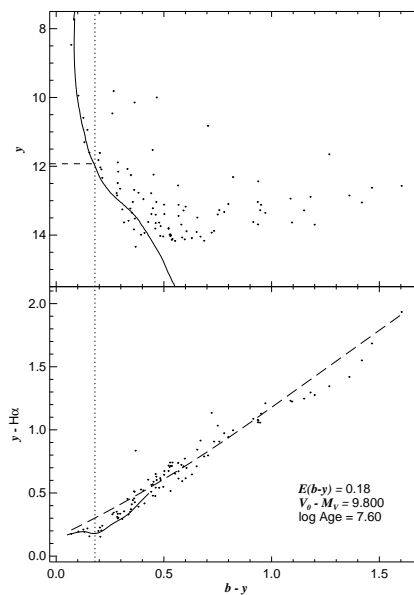


Fig. 36.— Color-magnitude (*top*) and color-color (*bottom*) diagrams of the cluster NGC 6178 in the same format as Figure 9.

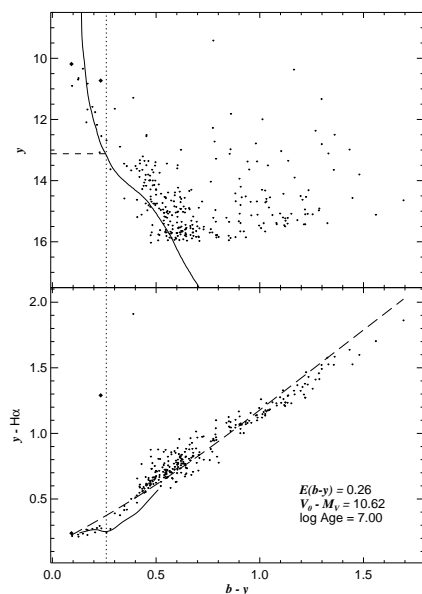


Fig. 35.— Color-magnitude (*top*) and color-color (*bottom*) diagrams of the cluster NGC 5593 in the same format as Figure 9.

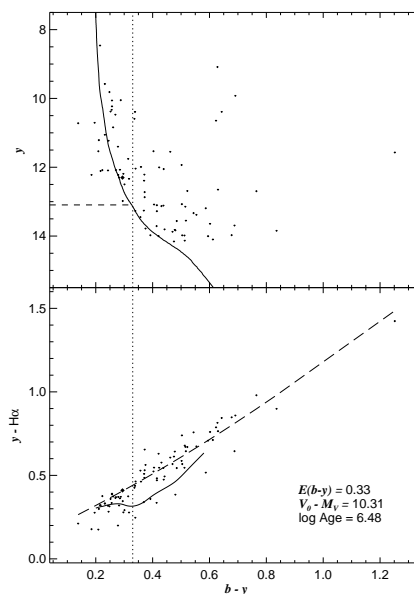


Fig. 37.— Color-magnitude (*top*) and color-color (*bottom*) diagrams of the cluster NGC 6193 in the same format as Figure 9.

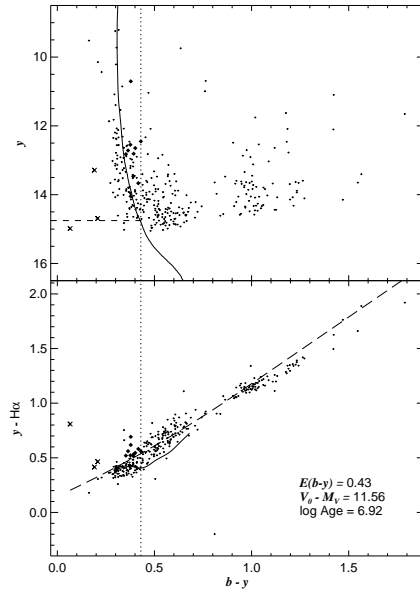


Fig. 38.— Color-magnitude (*top*) and color-color (*bottom*) diagrams of the cluster NGC 6200 in the same format as Figure 9.

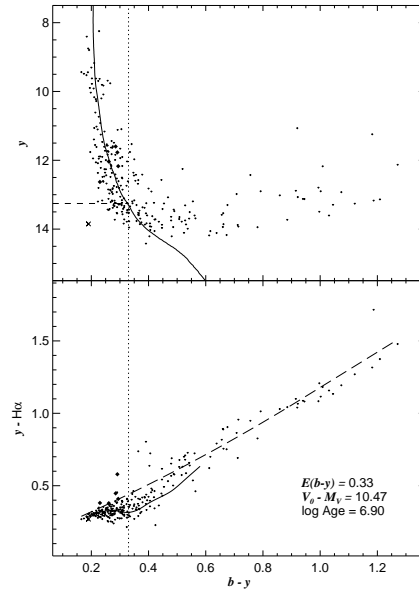


Fig. 40.— Color-magnitude (*top*) and color-color (*bottom*) diagrams of the cluster NGC 6231 in the same format as Figure 9.

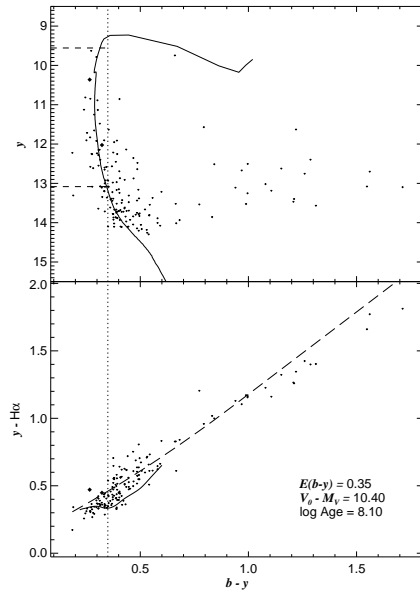


Fig. 39.— Color-magnitude (*top*) and color-color (*bottom*) diagrams of the cluster NGC 6204 in the same format as Figure 9.

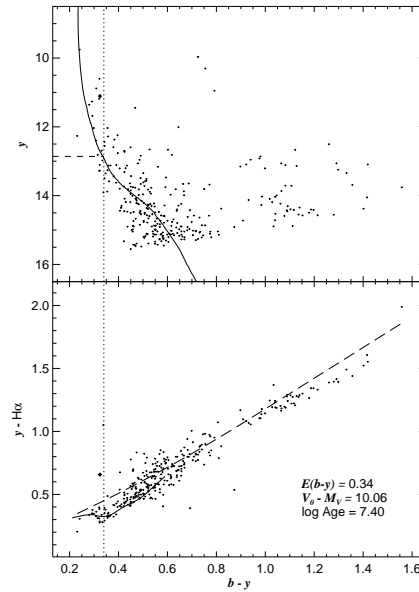


Fig. 41.— Color-magnitude (*top*) and color-color (*bottom*) diagrams of the cluster NGC 6249 in the same format as Figure 9.

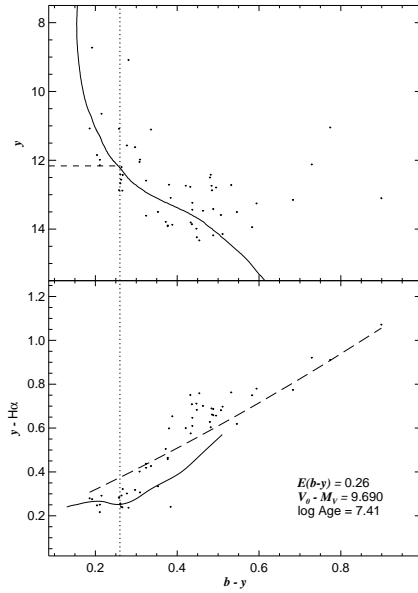


Fig. 42.— Color-magnitude (*top*) and color-color (*bottom*) diagrams of the cluster NGC 6250 in the same format as Figure 9.

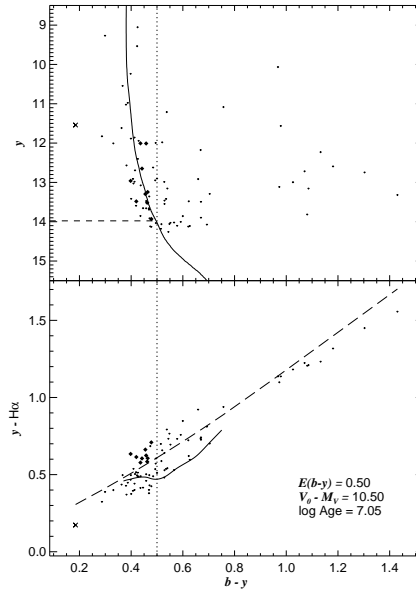


Fig. 44.— Color-magnitude (*top*) and color-color (*bottom*) diagrams of the cluster NGC 6322 in the same format as Figure 9.

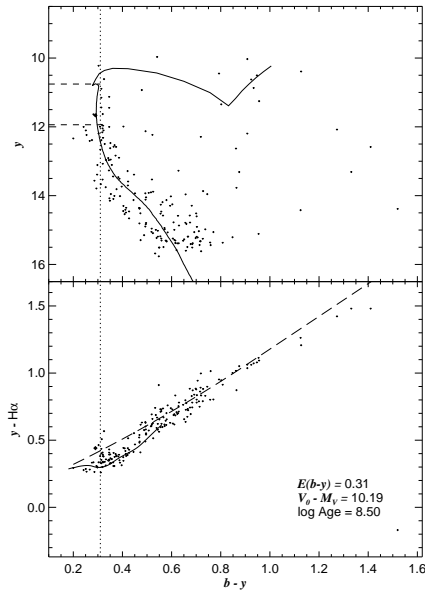


Fig. 43.— Color-magnitude (*top*) and color-color (*bottom*) diagrams of the cluster NGC 6268 in the same format as Figure 9.

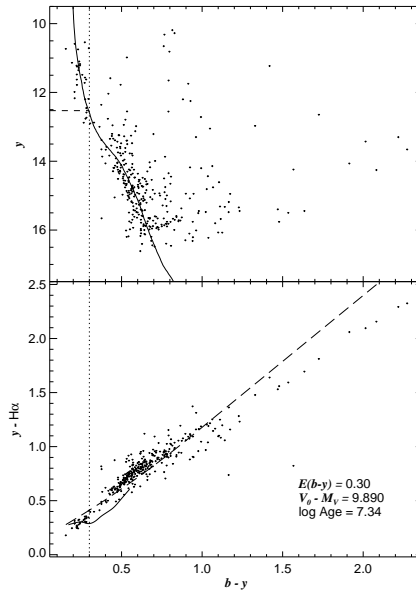


Fig. 45.— Color-magnitude (*top*) and color-color (*bottom*) diagrams of the cluster NGC 6425 in the same format as Figure 9.



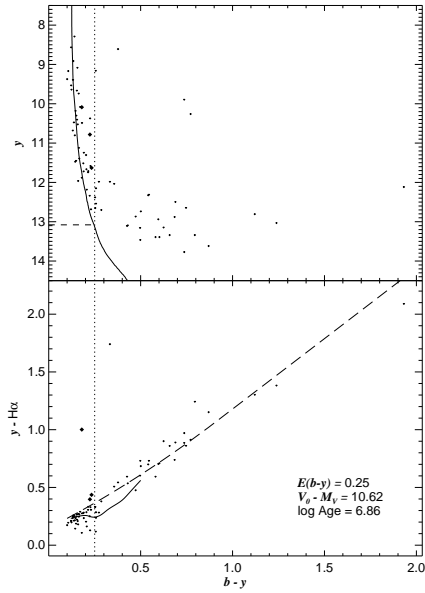


Fig. 46.— Color-magnitude (*top*) and color-color (*bottom*) diagrams of the cluster NGC 6530 in the same format as Figure 9.

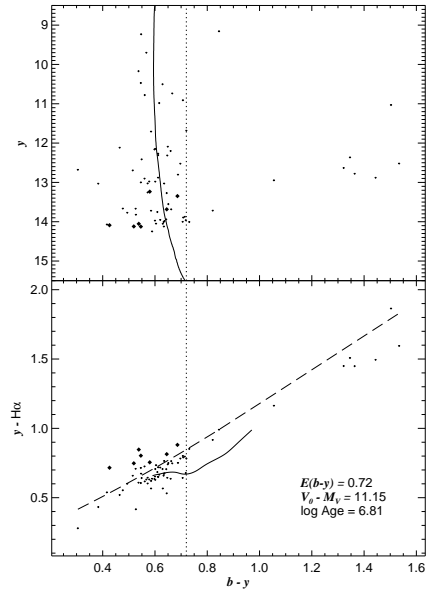


Fig. 48.— Color-magnitude (*top*) and color-color (*bottom*) diagrams of the cluster NGC 6604 in the same format as Figure 9.

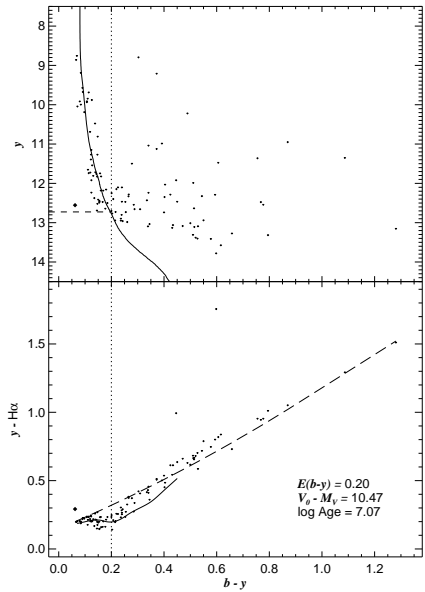


Fig. 47.— Color-magnitude (*top*) and color-color (*bottom*) diagrams of the cluster NGC 6531 in the same format as Figure 9.

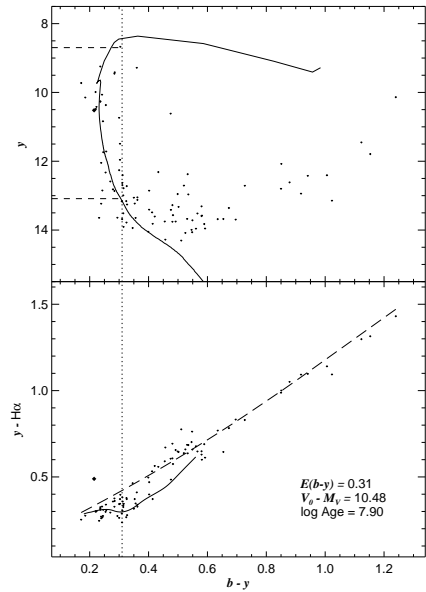


Fig. 49.— Color-magnitude (*top*) and color-color (*bottom*) diagrams of the cluster NGC 6613 in the same format as Figure 9.

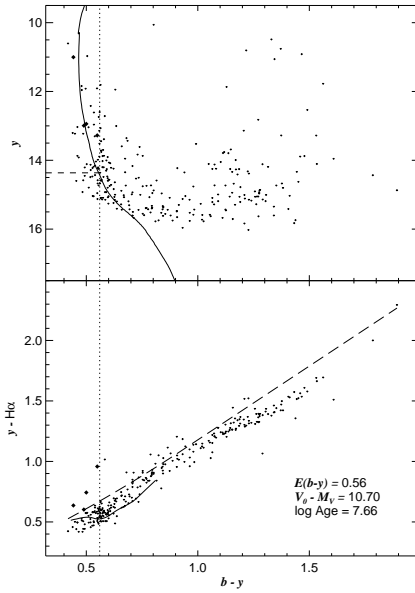


Fig. 50.— Color-magnitude (*top*) and color-color (*bottom*) diagrams of the cluster NGC 6664 in the same format as Figure 9.

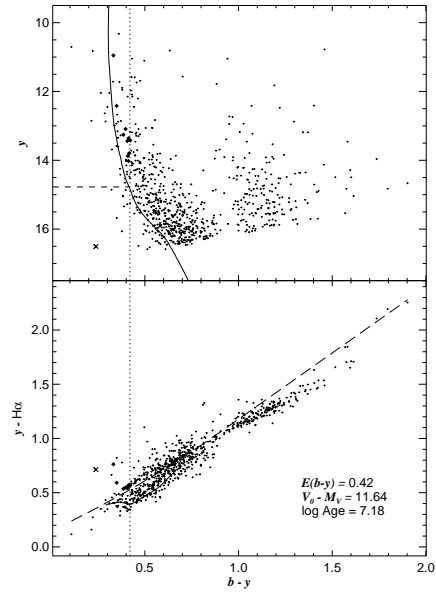


Fig. 52.— Color-magnitude (*top*) and color-color (*bottom*) diagrams of the cluster Ruprecht 119 in the same format as Figure 9.

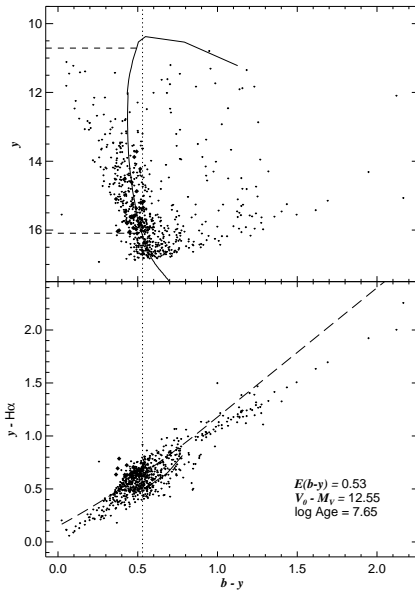


Fig. 51.— Color-magnitude (*top*) and color-color (*bottom*) diagrams of the cluster Ruprecht 79 in the same format as Figure 9.

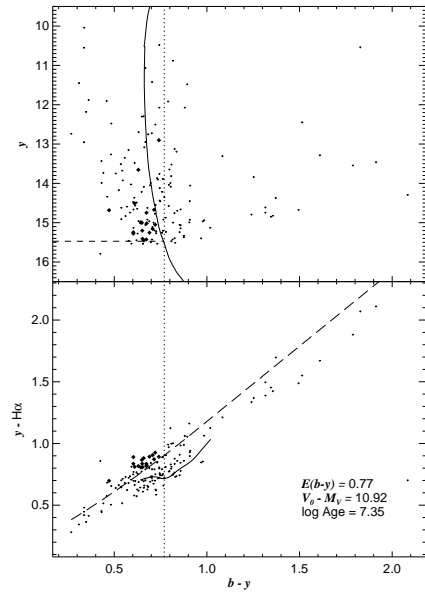


Fig. 53.— Color-magnitude (*top*) and color-color (*bottom*) diagrams of the cluster Ruprecht 127 in the same format as Figure 9.

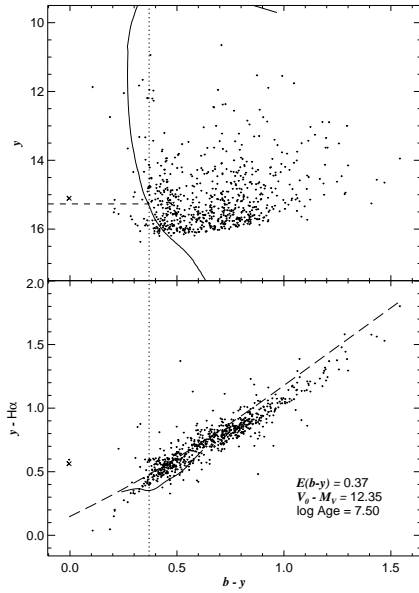


Fig. 54.— Color-magnitude (*top*) and color-color (*bottom*) diagrams of the cluster Ruprecht 140 in the same format as Figure 9.

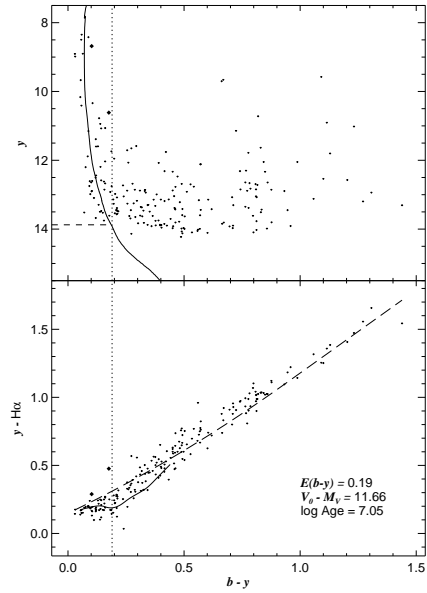


Fig. 56.— Color-magnitude (*top*) and color-color (*bottom*) diagrams of the cluster Stock 14 in the same format as Figure 9.

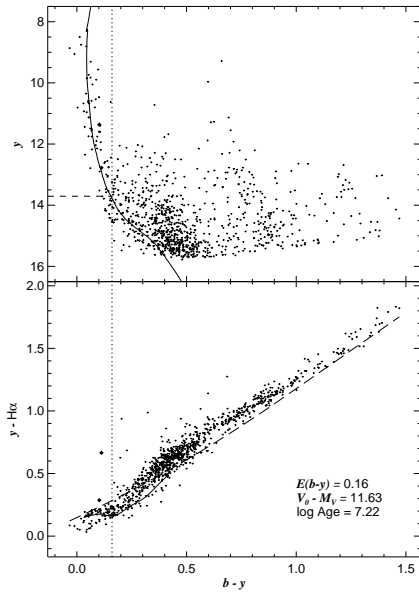


Fig. 55.— Color-magnitude (*top*) and color-color (*bottom*) diagrams of the cluster Stock 13 in the same format as Figure 9.

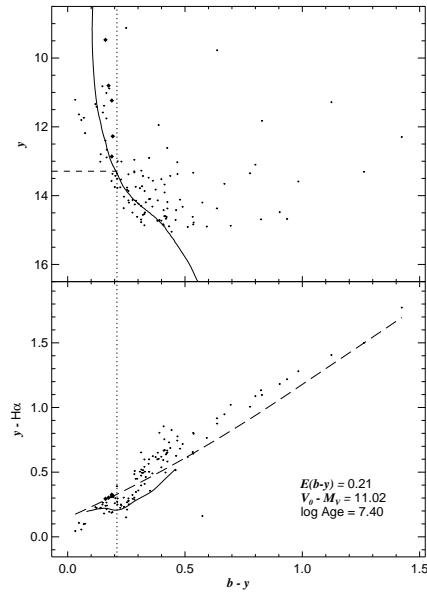


Fig. 57.— Color-magnitude (*top*) and color-color (*bottom*) diagrams of the cluster Trumpler 7 in the same format as Figure 9.

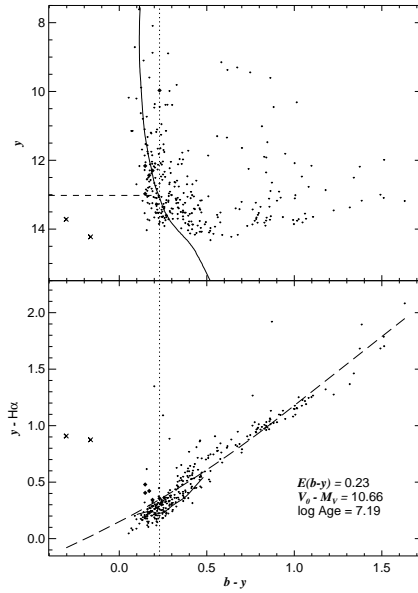


Fig. 58.— Color-magnitude (*top*) and color-color (*bottom*) diagrams of the cluster Trumpler 18 in the same format as Figure 9.

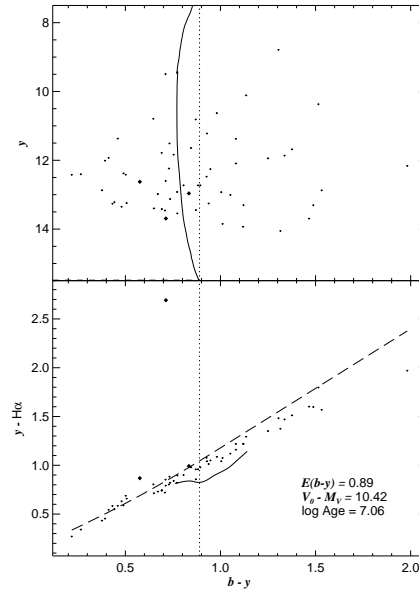


Fig. 60.— Color-magnitude (*top*) and color-color (*bottom*) diagrams of the cluster Trumpler 27 in the same format as Figure 9.

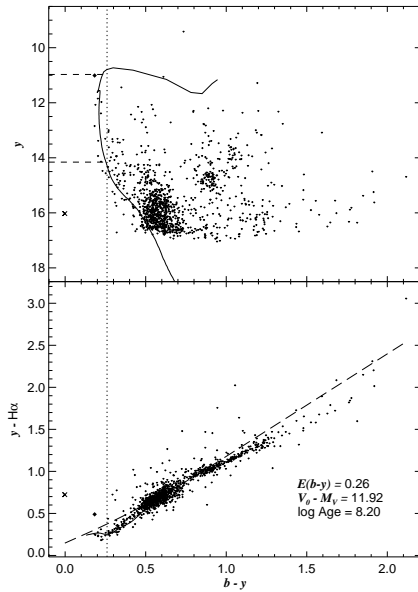


Fig. 59.— Color-magnitude (*top*) and color-color (*bottom*) diagrams of the cluster Trumpler 20 in the same format as Figure 9.

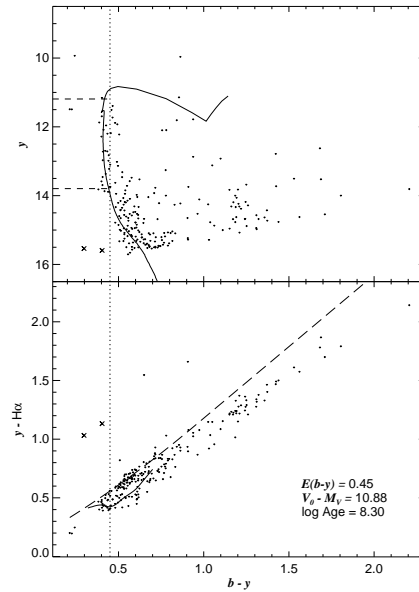


Fig. 61.— Color-magnitude (*top*) and color-color (*bottom*) diagrams of the cluster Trumpler 28 in the same format as Figure 9.

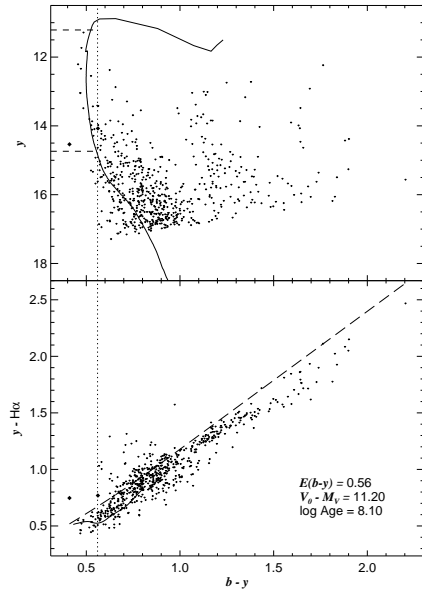


Fig. 62.— Color-magnitude (*top*) and color-color (*bottom*) diagrams of the cluster Trumpler 34 in the same format as Figure 9.

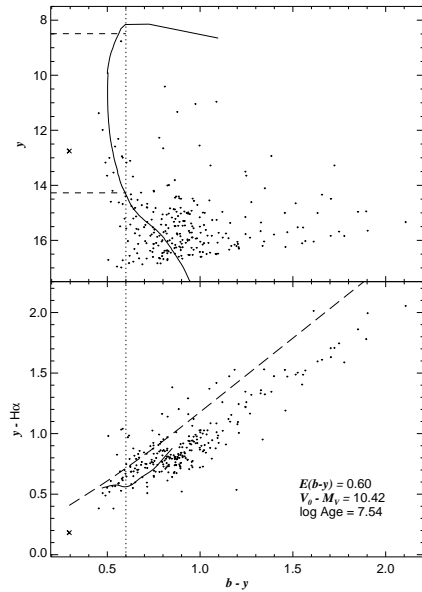


Fig. 63.— Color-magnitude (*top*) and color-color (*bottom*) diagrams of the cluster vdB-Hagen 217 in the same format as Figure 9.

TABLE 1  
PHOTOMETRY OF OPEN CLUSTERS

Cluster	No.	RA (2000)	Dec (2000)	$y$	$\delta y$	$b - y$	$\delta(b - y)$	$y - H\alpha$	$\delta(y - H\alpha)$	Code	WEBDA	Identifier
Basell	1	18 47 56.08	-5 45 51.0	16.445	0.066	0.988	0.103	0.917	0.103	O	...	...
Basell	2	18 48 01.11	-5 45 50.7	15.981	0.056	0.744	0.084	0.770	0.094	O	...	...
Basell	3	18 48 23.49	-5 45 50.9	16.137	0.060	0.868	0.092	0.876	0.098	O	...	...
Basell	4	18 48 33.34	-5 45 53.7	16.570	0.069	0.770	0.102	0.898	0.114	O	...	...
Basell	5	18 48 06.99	-5 45 55.7	14.437	0.050	1.396	0.079	1.537	0.064	O	...	...
Basell	6	18 48 37.87	-5 45 53.8	15.479	0.048	0.657	0.070	0.693	0.081	O	...	...
Basell	7	18 47 52.85	-5 45 56.7	16.315	0.064	0.868	0.096	1.037	0.096	O	...	...
Basell	8	18 48 01.30	-5 45 57.1	14.802	0.047	1.111	0.074	1.181	0.066	O	...	...
Basell	9	18 48 31.17	-5 45 56.8	15.899	0.054	0.812	0.084	0.683	0.093	O	...	...
Basell	10	18 48 34.64	-5 45 56.7	13.519	0.031	0.429	0.046	0.395	0.052	O	...	...

NOTE.—The complete version of this table is in the electronic edition of the Journal. For each star observed, we give the cluster name and our identifying number, the right ascension (RA), and declination (Dec) for the epoch 2000. We also provide the  $y$  magnitude, the  $b - y$  and  $y - H\alpha$  colors, and the error for each. The code is used to label definite Be stars (Be), possible Be stars (Be?), B-type stars (B), probable foreground stars (F), and other stars in the field (O). Finally, the WEBDA number and other identifiers are provided where available.

TABLE 2  
SUMMARY OF OPEN CLUSTERS

Cluster	RA (2000)	Dec (2000)	$E(b-y)$	$V_0 - M_V$	log Age	$N_{Be}$ (Definite)	$N_{Be}$ (Possible)	$N_{B+Be}$	References
Basel 1	18 48 12	-05 51 00	0.33	11.00	8.45	0	0	3	6
Bochum 13 <sup>a</sup>	17 17 24	-35 33 00	0.64	10.16	6.82	2	1	> 23	1
Collinder 272	13 30 26	-61 19 00	0.34	11.55	7.11	3	5	91	1,30
Haffner 16	07 50 20	-25 28 00	0.13	12.50	7.08	0	1	19	1,7,14
Hogg 16	13 29 18	-61 12 00	0.31	11.00	7.05	0	1	35	1
Hogg 22	16 46 37	-47 05 00	0.47	11.75	6.70	0	1	> 22	8,14
IC 2395	08 42 37	-48 06 48	0.05	9.24	7.22	0	1	14	1
IC 2581	10 27 24	-57 38 00	0.31	12.00	7.14	2	8	117	1,13,14
IC 2944 <sup>b</sup>	11 38 20	-63 22 22	0.24	11.27	6.82	1	2	50	1
NGC 2343	07 08 18	-10 39 00	0.11	10.12	8.00	0	0	11	1,11,14
NGC 2362	07 18 48	-24 57 00	0.07	10.71	6.91	0	1	41	1
NGC 2367	07 20 06	-21 53 00	0.26	11.84	6.74	0	3	16	1,7,31
NGC 2383	07 24 41	-20 56 42	0.20	12.62	7.40	2	0	20	14,26,31
NGC 2384	07 25 12	-21 01 24	0.22	11.63	6.90	0	2	33	1,31
NGC 2414 <sup>b</sup>	07 33 11	-15 27 12	0.41	11.99	6.80	5	13	86	14,31
NGC 2421	07 36 18	-20 37 00	0.35	11.69	7.40	4	6	65	1,14,16
NGC 2439 <sup>b</sup>	07 40 48	-31 39 00	0.30	12.18	7.25	6	7	111	1,14
NGC 2483 <sup>b</sup>	07 55 54	-27 56 00	0.30	12.31	7.00	2	10	49	14
NGC 2489	07 56 12	-30 04 00	0.30	10.81	8.38	0	0	7	14,19
NGC 2571	08 18 54	-29 44 00	0.10	10.64	7.49	1	0	24	1
NGC 2659	08 42 36	-44 57 00	0.38	10.80	6.89	1	4	32	1,27
NGC 3293	10 35 49	-58 13 00	0.22	12.20	6.90	3	8	> 91	4
NGC 3766	11 36 13	-61 36 55	0.15	11.40	7.16	5	8	> 146	1,25
NGC 4103	12 06 43	-61 15 21	0.22	11.70	7.35	1	2	92	23,33
NGC 4755	12 53 42	-60 22 00	0.28	11.80	6.85	5	7	> 178	3
NGC 5281	13 46 30	-62 54 54	0.19	11.00	7.71	1	5	40	14,15
NGC 5593	14 25 54	-54 49 00	0.26	10.62	7.00	1	1	15	34
NGC 6178	16 35 42	-45 38 00	0.18	9.80	7.60	0	0	6	15,21
NGC 6193 <sup>c</sup>	16 41 18	-48 46 00	0.33	10.31	6.48	0	1	31	1,10,15
NGC 6200	16 44 12	-47 29 00	0.43	11.56	6.93	2	8	112	1
NGC 6204	16 46 08	-47 00 44	0.35	10.40	8.10	0	2	34	5,8
NGC 6231 <sup>c</sup>	16 54 09	-41 49 36	0.33	10.47	6.90	2	3	129	1,20
NGC 6249	16 57 36	-44 47 00	0.34	10.06	7.40	1	0	13	14,15
NGC 6250	16 57 58	-45 56 36	0.26	9.69	7.41	0	0	7	1
NGC 6268	17 02 40	-39 44 18	0.31	10.19	8.50	1	0	2	22,34
NGC 6322 <sup>c</sup>	17 18 30	-42 56 00	0.50	10.50	7.06	1	8	43	1,18
NGC 6425	17 47 02	-31 30 00	0.30	9.89	7.35	0	0	25	1,29
NGC 6530 <sup>c</sup>	18 04 48	-24 20 00	0.25	10.62	6.87	1	2	> 41	1
NGC 6531	18 04 36	-22 30 00	0.20	10.47	7.07	1	0	49	1,9
NGC 6604 <sup>c</sup>	18 18 06	-12 14 00	0.72	11.15	6.81	0	7	> 63	1
NGC 6613	18 19 54	-17 08 00	0.31	10.48	7.90	1	0	29	12,14,34
NGC 6664	18 36 42	-08 13 00	0.56	10.70	7.66	2	2	36	24
Ruprecht 79 <sup>b</sup>	09 40 59	-53 51 00	0.53	12.55	7.65	1	31	288	1,28,32
Ruprecht 119	16 28 15	-51 30 00	0.42	11.64	7.18	1	9	50	1,22,34
Ruprecht 127 <sup>b</sup>	17 37 51	-36 18 00	0.77	10.92	7.35	0	18	97	1,18
Ruprecht 140 <sup>b</sup>	18 21 51	-33 13 00	0.37	12.35	7.50	0	1	25	34
Stock 13 <sup>c</sup>	11 13 05	-58 53 00	0.16	11.63	7.22	1	1	64	1,17
Stock 14	11 43 48	-62 31 00	0.19	11.66	7.06	1	1	47	1,14
Trumpler 7	07 27 22	-23 57 00	0.21	11.02	7.40	0	5	24	14
Trumpler 18	11 11 28	-60 40 00	0.23	10.66	7.19	0	5	71	1
Trumpler 20	12 39 34	-60 37 00	0.26	11.92	8.20	0	1	10	34
Trumpler 27 <sup>a</sup>	17 36 20	-33 31 00	0.89	10.42	7.06	1	2	> 34	1,29
Trumpler 28	17 37 00	-32 29 00	0.45	10.88	8.30	0	0	19	14,34
Trumpler 34	18 39 48	-08 25 00	0.56	11.20	8.10	1	1	18	34
vdB-Hagen 217	17 16 06	-40 49 00	0.60	10.42	7.54	0	0	12	2,34

<sup>a</sup>Cluster parameters unreliable.

<sup>b</sup>May not be a true cluster.

<sup>c</sup>May contain pre-MS Herbig Be stars.

References. — (1) WEBDA; (2) Ahumada et al. 2000; (3) Alfaro & Delgado 1991; (4) Baume et al. 2003; (5) Carraro & Munari 2004; (6) Delgado, Alfaro, & Cabrera-Cano 1997; (7) using mean values from FitzGerald et al. 1979; (8) Forbes & Short 1996; (9) Hagen 1970; (10) Herbst & Havlen 1977; (11) Kalirai et al. 2001; (12) Lindoff 1971; (13) Lloyd Evans 1969; (14) Lynga 1987; (15) Moffat & Vogt 1973; (16) Moffat & Vogt 1975a; (17) Moffat & Vogt 1975b; (18) Moffat & Vogt 1975c; (19) Paunzen & Maitzen 2001; (20) Perry, Hill, & Christodoulou 1991; (21) Piatti, Clariá, & Bica 2000a; (22) Piatti, Bica, & Clariá 2000b; (23) Sanner et al. 2001 (24) Schmidt 1982; (25) Shobbrook 1985; (26) Subramaniam & Sagar 1999; (27) Stetson 1981; (28) Tadross 2001; (29) Thé & Stokes 1970; (30) Vázquez et al. 1997; (31) Vogt & Moffat 1972; (32) Walker 1987; (33) Wesselink 1969; (34) this work.



TABLE 3  
CLUSTER MASS DISTRIBUTION

Cluster	$\Gamma$	$N_{tot}$	$N_{missing}$	$\Delta M^a (M_{\odot})$
Hogg 22 ..	$-1.11 \pm 0.27$	$49 \pm 10$	27	3.9 – 24.8
NGC 3293	$-1.00 \pm 0.14$	$189 \pm 21$	98	4.2 – 18.4
NGC 3766	$-1.67 \pm 0.10$	$191 \pm 9$	45	2.7 – 12.2
NGC 4755	$-1.04 \pm 0.13$	$247 \pm 17$	69	2.7 – 20.0
NGC 6530	$-0.68 \pm 0.34$	$66 \pm 7$	25	2.7 – 13.8
NGC 6604	$-1.27 \pm 0.19$	$127 \pm 18$	64	3.8 – 20.8

<sup>a</sup> $\Delta M$  represents the observed range of masses for the B stars in each cluster.

TABLE 4  
DISTRIBUTION OF OPEN CLUSTERS

Cluster	$\ell$ (deg)	$b$ (deg)	$d_{\odot}$ (kpc)	$d_{cent}$ (kpc)
Basel 1 . . . . .	27.36	-1.95	1.58	6.63
Collinder 272	307.62	1.25	2.04	6.94
Haffner 16 ..	242.08	0.48	3.16	9.88
Hogg 16 . . . . .	307.48	1.34	1.58	7.15
Hogg 22 . . . . .	338.56	-1.14	2.24	5.97
IC 2395 . . . . .	266.65	-3.58	0.70	8.07
IC 2581 . . . . .	284.60	0.01	2.51	7.76
IC 2944 . . . . .	294.85	-1.65	1.79	7.43
NGC 2343 ..	224.32	-1.14	1.06	8.79
NGC 2362 ..	238.18	-5.53	1.39	8.81
NGC 2367 ..	235.65	-3.84	2.33	9.51
NGC 2383 ..	235.26	-2.44	3.34	10.28
NGC 2384 ..	235.39	-2.41	2.12	9.37
NGC 2421 ..	236.24	0.08	2.18	9.39
NGC 2439 ..	246.42	-4.42	2.73	9.43
NGC 2489 ..	246.71	-0.78	1.45	8.68
NGC 2571 ..	249.11	3.54	1.34	8.57
NGC 2659 ..	264.16	-1.63	1.45	8.27
NGC 3293 ..	285.86	0.07	2.75	7.72
NGC 3766 ..	294.11	-0.03	1.91	7.43
NGC 4103 ..	297.58	1.15	2.19	7.25
NGC 4755 ..	303.21	2.53	2.29	7.01
NGC 5281 ..	309.17	-0.70	1.58	7.11
NGC 5593 ..	316.34	5.58	1.33	7.10
NGC 6178 ..	338.40	1.23	0.91	7.16
NGC 6193 ..	336.70	-1.57	1.15	6.96
NGC 6200 ..	337.99	-1.09	2.05	6.15
NGC 6204 ..	338.56	-1.03	1.20	6.89
NGC 6231 ..	343.46	1.19	1.24	6.82
NGC 6249 ..	341.55	-1.16	1.03	7.03
NGC 6250 ..	340.68	-1.93	0.87	7.19
NGC 6268 ..	346.10	1.22	1.09	6.95
NGC 6322 ..	345.29	-3.07	1.26	6.79
NGC 6425 ..	357.97	-1.59	0.95	7.05
NGC 6530 ..	6.14	-1.38	1.33	6.68
NGC 6531 ..	7.71	-0.44	1.24	6.77
NGC 6604 ..	18.26	1.69	1.70	6.41
NGC 6613 ..	14.15	-1.01	1.25	6.80
NGC 6664 ..	23.95	-0.49	1.38	6.76
Ruprecht 119	333.27	-1.90	2.13	6.17

TABLE 4—*Continued*

Cluster	$\ell$ (deg)	$b$ (deg)	$d_{\odot}$ (kpc)	$d_{cent}$ (kpc)
Stock 13 . . . . .	290.52	1.57	2.12	7.52
Stock 14 . . . . .	295.24	-0.64	2.15	7.35
Trumpler 7 . . . .	238.28	-3.38	1.60	8.95
Trumpler 18 ..	290.98	-0.14	1.36	7.62
Trumpler 20 ..	301.49	2.24	2.42	7.04
Trumpler 28 ..	355.99	-0.27	1.50	6.50
Trumpler 34 ..	24.09	-1.28	1.74	6.45
vdB-Hagen 217	346.76	-1.48	1.21	6.82

TABLE 5  
B STAR ROTATIONAL VELOCITIES

Spectral Type	$M_B$ ( $M_\odot$ )	$R_B$ ( $R_\odot$ )	$v_{crit}$ ( $\text{km s}^{-1}$ )	$\langle v \sin i \rangle$ ( $\text{km s}^{-1}$ )	$\langle v \sin i \rangle / v_{crit}$
B1 .....	13.5	5.9	560	127	0.23
B4 .....	5.2	3.2	470	108	0.23
B7 .....	3.5	2.5	440	152	0.35
B9 .....	2.4	2.1	390	134	0.34